Charles University in Prague
Faculty of Mathematics and Physics

DOCTORAL THESIS

Milan Aftanas

Thomson Scattering Diagnostic on COMPASS Tokamak

Department of Surface and Plasma Science

Supervisor of the doctoral thesis: RNDr. Jan Stöckel, CSc.
Study programme: Physics
Specialization: Physics of Plasmas and Ionized Media

Prague 2015

I would like to say big thank you to Prof. RNDr. Jana Šafránková, DrSc. and my supervisors, RNDr. Jan Stöckel, CSc. for their inexhaustible patience and responsive attitude. My next thanks is devoted to Dr. Michael Walsh and Dr. Rory Scannell for their selfless help and for their advices. I would like to thank Ing. Petr Böhm, Ph.D., RNDr. Petra Bílková, Ph.D., Mgr. Josef Havlíček and Mgr. Estera Štefániková for their support and lots of help. I am grateful to my collaborators in both the Institute of Plasma Physics AS CR, v.v.i. and the Charles University in Prague: Ing. Martin Hron, Ph.D., Mgr. Vladimír Weinzettl, Ph.D., Ing. Martin Imríšek, Ing. Jaroslav Krbec, Mgr. Jan Pipek, Mgr. Matěj Peterka and many others. Thank you to everyone at Institute of Plasma Physics AS CR, v.v.i. for making it a fun and interesting place to work over the last years. I feel fortunate to have had the opportunity to work with so many acomplished scientists during my PhD. Last but not least thanks to my parents, my brother and my friends for their support.

I declare that I carried out this doctoral thesis independently, and only with the cited sources, literature and other professional sources.

I understand that my work relates to the rights and obligations under the Act No. 121/2000 Coll., the Copyright Act, as amended, in particular the fact that the Charles University in Prague has the right to conclude a license agreement on the use of this work as a school work pursuant to Section 60 paragraph 1 of the Copyright Act.

In ..... date ..... signature of the author

Název práce: Diagnostika Thomsonovým rozptylem na tokamaku COMPASS

Autor: Milan Aftanas

Katedra: Katedra fyziky povrchů a plazmatu

Vedoucí disertační práce: RNDr. Jan Stöckel, CSc., Ústav fyziky plazmatu AV ČR, v. v. i.

Abstrakt: Detailní studium chování a parametrů plazmatu je důležitou částí fúzního výzkumu. Diagnostiky poskytující spolehlivé měření jsou pro snahu o kontrolu fúzní energie na Zemi klíčové. Diagnostika Thomsonovým rozptylem je náročnou, avšak spolehlivou a nezastupitelnou částí diagnostického aparátu většiny zařízení pro studium magnetického udržení vysokoteplotního plazmatu pro její schopnost měřit elektronovou hustotu a absolutní hodnoty elektronové teploty s velkým prostorovým rozlišením. Má práce se věnuje této diagnostice pro tokamak COMPASS počínaje jejím návrhem, přes technické zpracování až po zpracování dat a analýzu chování plazmatu. Podílel jsem se též na návrhu diagnostiky Thomsonovým rozptylem pro tokamak ITER, a v práci je jí věnována jedna kapitola.

Klíčová slova: tokamak, Thomsnův rozptyl, fúze, COMPASS

Title: Thomson Scattering Diagnostic on COMPASS Tokamak

Author: Milan Aftanas

Department: Department of Surface and Plasma Science

Supervisor: RNDr. Jan Stöckel, CSc., Institute of Plasma Physics CAS, v.v.i.

Abstract: Thorough study of plasma behaviour in magnetically confined fusion devices is of great importance in recent research. Diagnostics capable to reliably provide important parameters of the hot plasma are key tool in the effort to control fusion energy on Earth. Thomson Scattering diagnostic has a credit of being a complex design diagnostic with reliable measurement of electron temperature and density profiles. The main subjects of this thesis are design of the Thomson Scattering system for the COMPASS tokamak, analysis of output data errors and exploitation of the data to study plasma behaviour. Besides this work, the author has been involved in the design of Thomson Scattering systems for the ITER tokamak and this design is presented here as well.

Keywords: tokamak, Thomson Scattering, fusion, COMPASS

Contents

1. Introduction

As mankind, we look for the ways how to ensure an energy for future. Nuclear fusion reaction, the energy source of stars, has been one of the candidates to fulfil this role from its early discovery.

1.1 Fusion

Fusion reactions are nuclear reaction of two or more atom nuclei. To fuse, significant amount of kinetic energy is needed to overcome strong electrostatic Coulomb force which causes protons to repel each other. Product of such reaction is atom with higher number of nuclei. Matter is not conserved in this reaction and it is converted from/into energy through:

$$E = mc^2 \tag{1.1}$$

For light atoms the reaction is exothermic and releases energy. For heavy atoms the reaction is endothermic and requires the external energy. This behaviour of releasing/requiring energy can be described with binding energy (Figure 1.1), which is the energy required to disassemble the atom to separate parts (nuclei).

Issue of nuclear fusion reactors is reaching and sustaining conditions in which the strong repulsive forces of the particles are overcome and nuclear fusion reaction can be maintained. General measure of the conditions to reach fusion ignition, known as Lawson criterion, has been described by John D. Lawson in 1955 [4]. The ignition is defined as an energy balance of plasma heating and losses. Lawson criterion gives a minimum required plasma density n and the energy confinement time τ_E, which measures the rate of energy losses, as:

$$n \cdot \tau_E \geq \frac{12}{E_{chp}} \frac{3nk_bT}{\langle \sigma v \rangle}, \tag{1.2}$$

where E_{chp} is energy of charged fusion products (in case of deuterium-tritium reaction is equal to 3.5 MeV), k_b is Boltzmann constant. Reaction cross section σ determines the likelihood of the reaction for the case of one nuclei striking another one. This probability depends on relative velocity v of incident particles/nuclei. $\langle\rangle$ means an average over velocity distribution function at temperature T. For the deuterium-tritium reaction the minimum (Figure 1.2), which occurs near $T = 25$ keV, can be written as:

$$n \cdot \tau_E \geq 1.5 \cdot 10^{20}\ s \cdot m^3 \tag{1.3}$$

1.2 Tokamak

One approach to control the nuclear fusion on the Earth is magnetic confinement, which stands for trapping plasma in a magnetic field to increase the left side of the Lawson criterion formula Equation 1.2 (energy confinement time form). One

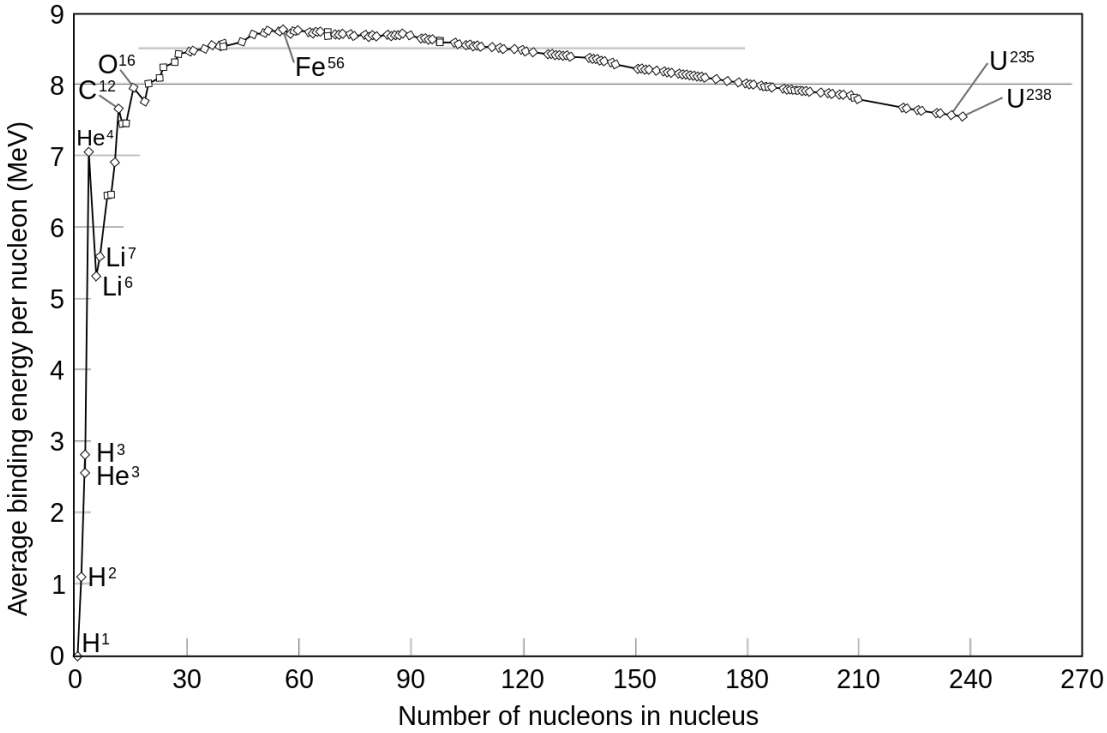

Figure 1.1: Average binding energy per nucleon for common isotopes with mark of few important atoms. Iron (Fe) with 56 nuclei is the most stable (highest binding energy) known atom. Nuclear reaction which creates product of higher binding energy is exothermic, and via versa. `http://en.wikipedia.org/wiki/Fusion_power`

of the most promising magnetic confinement device is tokamak (abbreviation of Russian: 'toroidal chamber with magnetic coils'). The concept of the device has been invented in the 1950s by Soviet physicists Andrei Sakharov and Igor Tamm (based on idea of Oleg Lavrentiev). Idea of the tokamaks is on the one hand generation of toroidal magnetic field by external coils (toroidal coils) and on the other shaping helical magnetic field lines by the flow of plasma current (which is transformer induced). Apart from toroidal coils, tokamak requires poloidal coils to control the position and the shape of the plasma (see Figure 1.3).

1.3 Tokamak COMPASS

The COMPASS (COMPact ASSembly) tokamak was originally operated in UKAEA Culham, United Kingdom, and it has been re-installed in the Institute of Plasma Physics (IPP) of the Academy of Sciences of the Czech Republic in Prague, Czech Republic at 2006 [11]. It is an ITER-like plasma cross-section device ($R = 0.56$ m, $a = 0.2$ m) operated in a divertor plasma configuration [7]. Table 1.1 summarizes the main parameters of the device.

Aside from main COMPASS parts as the vacuum chamber, magnetic field coils and tokamak support structure, all the auxiliary systems like power supplies, cooling, vacuum, Control, Data Acquisition and Communication system (CODAC) [3] and most of the diagnostics [12] were newly developed for the re-installation in Prague.

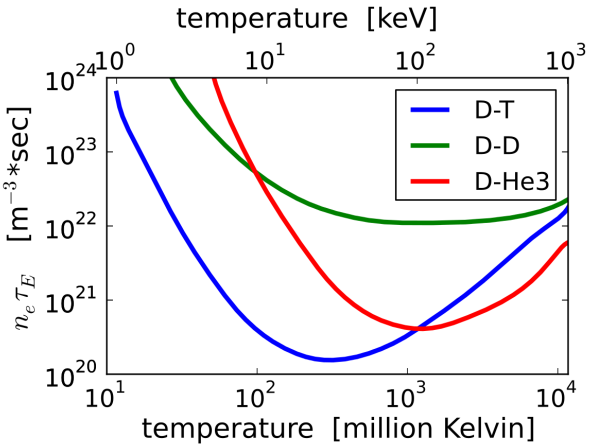

Figure 1.2: Lawson criterion for the three fusion reactions (deuterium-tritium, deuterium-deuterium, deuterium-helium3). `https://en.wikipedia.org/wiki/Lawson_criterion`

Major radius	0.56 m
Minor radius	0.2 m
Plasma current	< 400 kA
Magnetic field	$0.8 - 2.1$ T
Triangularity	0.5
Elongation	< 1.8
Pulse length	< 1 s
NBI system	2x 0.35 MW

Table 1.1: Summary of COMPASS parameters

During years 2008 and 2009 the COMPASS tokamak was running in a test operation and commissioning of all the new systems and diagnostics. Within another 2 years the full performance has been achieved, namely H-mode scenarios in ITER-relevant geometry. Scientific work relevant to current fusion research has started in 2012 when the full performance and the Type-I ELMy H-mode operational scenario has been successfully achieved. The COMPASS tokamak has been equipped with additional systems which help to fulfil the scientific goal: flexible plasma heating system of Neutral Beam Injectors (NBIs) and Edge Localized mode (ELM) control systems. Two new NBIs, operating either in co- or counter-injection configuration, are able to provide power of 700 kW (2x 350 kW) at the beam energy of 40 keV. The new ELM control systems - vertical kicks system and Resonant Magnetic perturbation system - uses the existing saddle coils mounted on vacuum vessel. Figure 1.4 shows cross-section size comparison with the main european tokamaks.

The scientific programme goal is to provide data for physics scaling towards ITER - together with ASDEX Upgrade and JET (Figure 1.4). It focuses primarily on the edge plasma, Scrape-off-Layer and divertor. Fundamental topics are understanding of plasma interaction with magnetic perturbations, power-fluxes decay lengths in SOL and divertor, role of GAMs and Zonal flows, effect of isotopes on the L-H transition, etc. All new diagnostics on the COMPASS tokamak

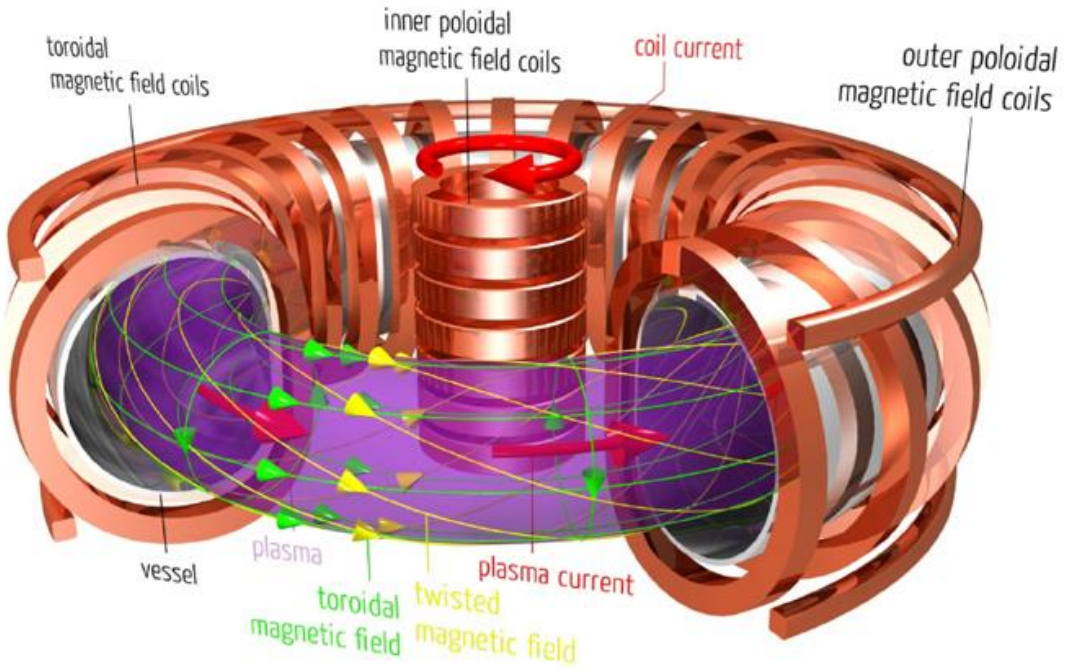

Figure 1.3: Tokamak schematic layout. https://en.wikipedia.org/wiki/Tokamak

provide unique spatial and temporal resolution to reflect these studies.

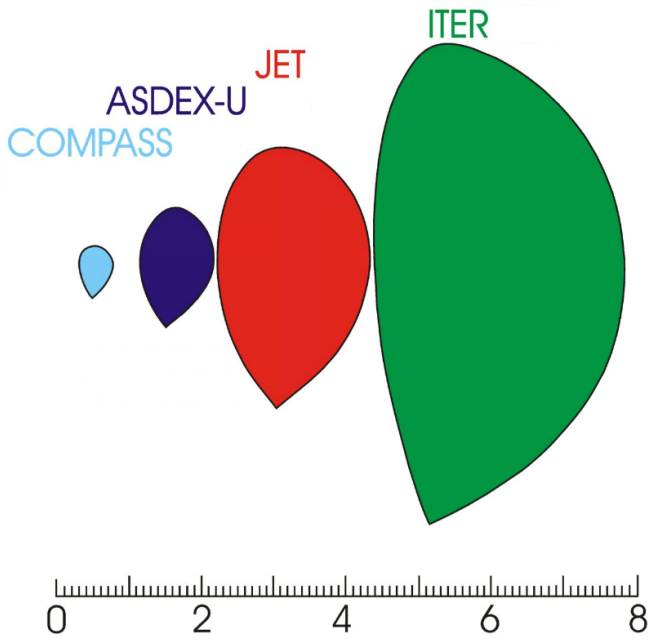

Figure 1.4: Size comparison of COMPASS, Asdex-U, JET and ITER tokamak.

2. Thomson scattering theory

Thomson scattering (TS) is a process of scattering of electromagnetic waves on free electrons or ions in the plasma. On the COMPASS tokamak, a laser beam with wavelength $\lambda = 1064$ nm is used. Waves spread in plasma without significant losses or change of frequency. This process will be described on free electrons (analogical equations could be derived also for the case of free ions) as it is used on majority of fusion devices with TS diagnostics. The TS based on scattering on free ions is a much more challenging diagnostics.

When incident electromagnetic wave with frequency ω_i interact with free electron in plasma, the electron is accelerated and starts to oscilate with the same frequency and emits electromagnetic radiation. The plasma electrons are im motion and therefore the effect of Doppler shift occurs. The electrons move with respect to the source as well as with respect to the observer, the resulting radiation then has double Doppler shift and the measured spectrum is broadened. From the energy and momentum conservation law, the equation for energy $E_p - E_p^{'}$, given to the electron by the incident photon with energy E_p, can be derived:

$$E_p - E_p^{'} = \left(\frac{E_p^2}{m_{0e}c^2}\right) \frac{1 - cos\varphi}{1 + \frac{E_p}{m_{0e}c^2}(1 - cos\varphi)}, \tag{2.1}$$

where $E_p^{'}$ is the energy of electron after the collision, $m_{0e}c^2$ is the rest mass of the electron and the angle φ corresponds to the deflection of the photon from its original trajectory. In real diagnostic setting, where $E_p \approx 1$ eV, $m_{0e}c^2 = 511$ eV and therefore $m_{0e}c^2 \gg E_p$, the electromagnetic wave does not have a significant influence on the trajectory of the electron and the change in electron's energy and momentum is negligible. This makes a huge advantage from a diagnostic point of view, putting TS in a non-invasive plasma diagnostics cathegory.

2.1 Acceleration of an electron

In this section, the acceleration of an electron by incident electromagnetic wave will be derived, as the radiation emitted by accelerated electron is proportional to $\vec{v}^3$. Relativistic effects have to be included into derivation, because for the typical reached temperatures in tokamaks ~ 5 keV, the estimation of particle velocities v using $E_k = \frac{1}{2}m_{0e}v^2$ gives the approximate value of $0.15c$, where c is the speed of light. Moreover, considering the temperatures which will be reached on next step fusion devices like ITER, where $T_e \approx 40\ keV$ ($v \approx 0.4c$), the relativistic effects will play even stronger role in the process of TS.

For the derivation the Newton equation of motion will be used ([9]), considering the relativistic mass of electron m with rest mass m_{0e} on the left hand side and the Lorentz force acting on the electron with charge e and velocity $\vec{v}$ by the incident wave with electric $\vec{E_i}$ and magnetic $\vec{B_i}$ component on the right hand side:

$$\frac{dm\vec{v}}{dt} = \frac{d}{dt}\left(\frac{m_{0e}\vec{v}}{\sqrt{1 - \frac{v^2}{c^2}}}\right) = -e(\vec{E_i} + \vec{v} \times \vec{B_i}) \tag{2.2}$$

After introducing new variables $\vec{\beta} = \vec{v}/c$, $\dot{\vec{\beta}} = \dot{\vec{v}}/c$, $\gamma = \left(1 - \frac{v^2}{c^2}\right)^{-1/2}$ and performing the derivative, a new equation is obtained:

$$m_0\gamma\dot{\vec{\beta}} + m_0\gamma^3\vec{\beta}(\vec{\beta}\cdot\dot{\vec{\beta}}) = -e\left(\frac{\vec{E}_i}{c} + \vec{\beta}\times\vec{B}_i\right). \tag{2.3}$$

A scalar multiplication with $\vec{\beta}$ can be applied on the equation above to obtain the term in bracket on the left hand side, using the vector identity $\vec{\beta}\cdot(\vec{\beta}\times\vec{B}_i) = 0$, obtaining

$$\vec{\beta}\cdot\dot{\vec{\beta}} = -\frac{e}{m_{0e}\gamma^3 c}\vec{\beta}\cdot\vec{E}_i \tag{2.4}$$

which can be inserted to the previous equation. By applying basic knowledge from the theory of electromagnetism as $\vec{B} = \frac{1}{c}\hat{i}\times\vec{E}$, where $\hat{i}$ is the direction of propagation of the incident wave, and the double vector product, the resulting relation for the acceleration of the electron by incident electromagnetic wave is derived ([9]):

$$\dot{\vec{\beta}} = -\frac{e}{m_{0e}\gamma c}\left(\vec{E}_i - (\vec{\beta}\cdot\vec{E}_i)\vec{\beta} + \hat{i}(\vec{\beta}\cdot\vec{E}_i) - \vec{E}_i(\vec{\beta}\cdot\hat{i})\right). \tag{2.5}$$

As can be seen from this equation, when the electric field $\vec{E}_i$ is zero, also the acceleration is equal to zero. When the electron velocity is negligible compared to the speed of light, the electron is given acceleration equal to $-\frac{e}{m_{0e}c}\vec{E}_i$ in the direction of the incident wave given by the first term of the equation. The second term corresponds to the relativistic correction, while the rest corresponds to the contribution from the magnetic field $\vec{B}_i$.

2.2 Radiated power

For the purpose of derivation of the radiated power P, the relations for electromagnetic potentials ϕ and $\vec{A}$, also known as Lienhart-Wiechert potentials ([9], Appendix B and C), have to be introduced. They are written together with derived electric $\vec{E}_s$ and magnetic field $\vec{B}_s$ in a system of following equations:

$$\phi(\vec{r},t) = \frac{q}{4\pi\varepsilon_0}\left[\frac{1}{R - \vec{R}\cdot\vec{\beta}}\right]_{ret}, \tag{2.6}$$

$$\vec{A}(\vec{r},t) = \frac{\mu_0 q}{4\pi}\left[\frac{\vec{v}}{R - \vec{R}\cdot\vec{\beta}}\right]_{ret}, \tag{2.7}$$

$$\vec{E}_s(\vec{r},t) = \frac{q}{4\pi\varepsilon_0}\left[\frac{1}{\tilde{\kappa}^3 Rc}\hat{s}\times(\hat{s} - \vec{\beta})\times\dot{\vec{\beta}}\right]_{ret}, \tag{2.8}$$

$$\vec{B}_s(\vec{r},t) = \frac{1}{c}\hat{s}\times\vec{E}_s(\vec{r},t), \tag{2.9}$$

whereas the classical relations between the electromagnetic potentials and the fields used for the derivation of above expressions (e.g. [9], p.35-40) are the following:

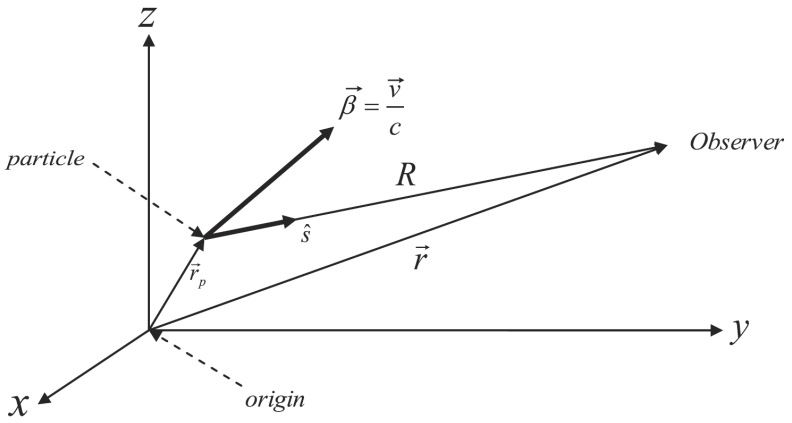

(a)

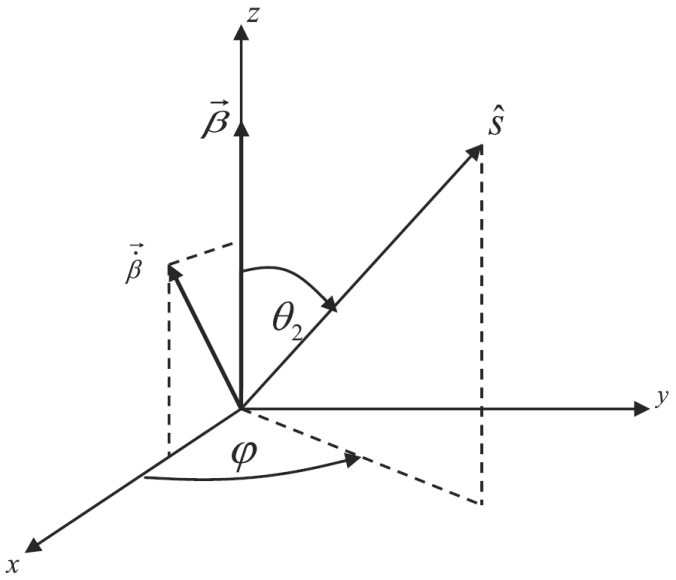

(b)

Figure 2.1: (a) Scattering coordinate system diagram, (b) The coordinate system to determine the total radiated power P_{tot} [9]

$$\vec{E} = -\nabla\phi - \frac{\partial\vec{A}}{\partial t} \tag{2.10}$$

$$\vec{B} = \nabla \times \vec{A}. \tag{2.11}$$

The meaning of some of the quantities $(\hat{s}, \vec{R}, R, \vec{r}, \vec{v}, \vec{\beta}, \dot{\vec{\beta}})$ is explained in the Figure 2.1(a), ε_0, μ_0, c are universal constants. $\tilde{\kappa}$ is defined as $\tilde{\kappa} = 1 - \vec{\beta}\cdot\hat{s} = 1 - \beta cos\theta_2$, using the notations from the Figure 2.1(b). The indexes $[]_{ret}$ used with some expressions means that the time dependent quantities are calculated in the so-called retarded time $t' = t - \frac{|\vec{r}-\vec{r_p}|}{c}$, $|\vec{r} - \vec{r_p}| = R$, that includes the time during which the light reaches the observer ([9]).

The power of electromagnetic field is defined by means of the Poynting vector $\vec{S_s}$:

$$\vec{S_s} = \vec{E_s} \times \vec{H_s}, \tag{2.12}$$

where $\vec{H_s}$ is defined using $\vec{B_s} = \mu_0 \vec{H_s}$. The Poynting vector represents the directional energy flux density of an electromagnetic field E through a surface dA in unit time, $d^2E = |\vec{S_s}|dAdt$. By integrating the Poynting vector over a sphere S, the total radiated power can be calculated:

$$P_{tot} = \int_S \vec{S_s} dA. \tag{2.13}$$

It is important to note that the radiated energy detected in point $\vec{r}$ was radiated during the time interval $dt^{'}$, not during dt. The time interval therefore has to be transformed as $dt = (1 - \vec{\beta} \cdot \hat{s})dt^{'}$ (the complete derivation can be found in [9]). The surface unit can be derived using the solid angle Ω as $dA = R^2 d\Omega$. By taking into account the equations in this subsection, the expression for radiated power can be obtained:

$$P = \frac{q^2}{16\pi^2 \varepsilon_0 c} \int \frac{|\hat{s} \times (\hat{s} - \vec{\beta}) \times \dot{\vec{\beta}}|^2}{(1 - \vec{\beta} \cdot \hat{s})^5} d\Omega, \tag{2.14}$$

from which the power radiated to the unit angle $dP/d\Omega$ can be estimated. Finally, the resulting expression for the total radiated power is stated below. The detailed derivation can be found in [9].

$$P_{tot} = \frac{q^2 \gamma^6}{6\pi c \varepsilon_0} \left[\dot{\beta}^2 - (\vec{\beta} \times \dot{\vec{\beta}})^2 \right] \tag{2.15}$$

The total radiated power is strongly dependent on γ with 6^{th} power, which increases with particle velocity. The more is a particle velocity approaching the speed of light, the stronger it radiates. A more detailed investigation of the angular distribution of P_{tot} has shown that the radiation is directed in the direction of motion $\vec{\beta}$ of the particle and gets stronger with increase of the velocity. This phenomena is also called the headlight effect ([9]).

2.3 Thomson scattering cross-section

The TS cross-section σ can be defined using the radiated power P_{tot} and the magnitude of the Poynting vector of the incident radiation S_{inc}:

$$P_{tot} = \sigma S_{inc} = \sigma c \varepsilon_0 E_i^2. \tag{2.16}$$

A small particle velocity ($\beta \ll 1$) is assumed. Then the term inside the integral in (Equation 2.14) is simplified to expression $\dot{\beta}^2 - (\dot{\vec{\beta}} \cdot \hat{s})^2$, which is possible to rewrite using angle θ_2 (see Figure 2.1(b)) to $\dot{\beta}^2(1 - cos^2\theta_2) = \dot{\beta}^2 sin^2\theta_2$. After inserting this into equation Equation 2.14, and integrating over solid angle $d\Omega = sin\theta_2 d\theta_2 d\varphi$, a new expression for P_{tot} is obtained ([9]):

$$P_{tot} = \frac{q^2 \dot{\beta}^2}{16\pi^2 c \varepsilon_0} \int_0^{2\pi} \int_0^{\pi} sin^3\theta_2 d\theta_2 d\varphi = \frac{8\pi}{3} \frac{q^4}{16\pi^2 c^4 \varepsilon_0^2 m_0^2} (\varepsilon_0 c E_i^2). \tag{2.17}$$

For obtaining this expression, a result from derivation of acceleration of the electron $\dot{beta}$ (Equation 2.5) for $\beta \ll 1$ is used. By comparing last two equations and assuming scattering on the electrons only ($q = e$), the expression for TS cross-section σ_{TS} is obtained:

$$\sigma_{TS} = \frac{8\pi}{3}\left(\frac{e^2}{4\pi\epsilon_0 m_{0e}c^2}\right)^2 = \frac{8\pi}{3}r_e^2 \tag{2.18}$$

where r_e is a standard definition of electron diameter ([9]). From the resulting equation, two following considerations can be made. First, the TS cross-section is extremely small, $\sigma_{TS} \simeq 6.65 \cdot 10^{-29}\ m^2$. It relates to the probability of the interactions, therefore the phenomenon of TS can be observed only with the interaction of the high power light beam with high free electron density medium (plasma). The only current source of such focused and intense radiation are high-powered lasers based on Q-switching. Another constraint is the fact that in the used TS diagnostic set-up, the scattered radiation is collected from relatively small solid angle, which further reduces the electron yield. Second fact resulting from the expression above is the indirect dependence of σ_{TS} on the scattering particles's mass. Therefore in this case, the scattering on the protons (which have approximately a thousand times greater mass) can be neglected, as the protons scatter 10^6 times less incoming power than the electrons under the same conditions. However, under some conditions, it is also possible to estimate the parameters of the ions in plasma by TS diagnostics. Such setting of the diagnostics is also based on measuring of the radiation scattered by electrons, the difference is in electron collective behaviour. Electrons form 'clouds' around positively charged ions, and their relative velocity is bound. Further explanation can be found in following section.

From Equation 2.14, a differential cross-section $d\sigma/d\Omega$ can be also derived, assuming non-relativistic velocities, where $\beta \gg 1$. It corresponds to the probability of the scattering to the unit solid angle. Using $\dot{\vec{\beta}}$ from Equation 2.5 for non-relativistic case, the resulting expression is obtained:

$$\frac{d\sigma}{d\Omega} = r_e^2 sin^2(\theta_2). \tag{2.19}$$

As can be seen, the probability of the scattering is angle dependent. The maximum scattering is observed, when angle θ_2 is equal to 90°. TS is therefore most effective in the plane perpendicular to the direction of polarization of the incident electromagnetic wave.

2.4 Scattered electric field in the standard TS geometry

In the standard TS geometry, the electric intensity vector $\vec{E_i}$ of an incident wave is perpendicular to the scattering plane given by $\hat{s}$ and $\hat{i}$ (see Figure 2.2), which implies $\hat{e} \cdot \hat{s} = 0 = \hat{e} \cdot \hat{i}$. For this case, the derivation of the electric field shape $\vec{E_s}$ (Equation 2.8) originated from the radiation of the electron with acceleration $\dot{\vec{\beta}}$ (Equation 2.5. To simplify, a placement of a polarizer of the scattered

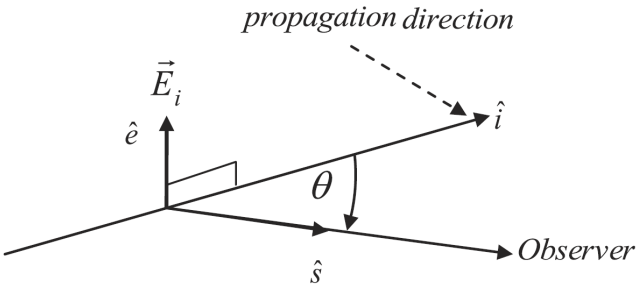

Figure 2.2: Plane defined by $\hat{i}$ and $\hat{s}$: the incident electric field $\vec{E_i}$ is perpendicular to the scattering plane, [9]

radiation can be assumed, such as only the contribution in the direction of the electric intensity of the incident wave $\vec{E_i}(\hat{e})$ will be collected. After providing the multiplication and using well-known vector identities, the following expression is obtained:

$$E_s(R,t) = \frac{e^2}{4\pi\varepsilon_0 m_{0e} c^2}\left[\frac{E_i}{\gamma(1-\beta_s)^3 R}((1-\beta i)(1-\beta_s) - \beta_e^2(1-cos\theta))\right]_{ret}, \tag{2.20}$$

where $\beta_s = \vec{\beta}\cdot\hat{s}$, $\beta_e = \vec{\beta}\cdot\hat{e}$, $\beta_i = \vec{\beta}\cdot\hat{i}$ and the angle θ is from the (Figure 2.2). The resulting expression corresponds to magnitude of the scattered electric field by single electron in the direction $\hat{e}$, where the electric field of the incident wave $\vec{E_i}$ is perpendicular to the scattering plane. Consider now a planar monochromatic wave incident on the electron in retarded time $t^{'}$:

$$E_i = E_{i0} cos(\vec{k_i}\cdot\vec{r_p}(t^{'}) - \omega_i t^{'}), \tag{2.21}$$

where $\vec{k_i}$ is the wave vector, ω_i is the angular frequency of the wave and E_{i0} is the initial amplitude. With the assumption that electron's trajectory is not strongly influenced by the incident wave (as mentioned at the beginning of this chapter), the position vector $\vec{r_p}(t^{'})$ is given by the expression $\vec{r_p}(t^{'}) = \vec{v}t^{'} + \vec{r}_{p0}$, where $\vec{r}_{p0}$ is vector of the initial position. A classic expression for the retarded time (**??**) can be modified using the Taylor expansion and expression for $\vec{r_p}(t^{'})$:

$$t^{'} = \frac{1 - \frac{R}{c} + \frac{\hat{s}\cdot\vec{r}_{p0}}{c}}{1 - \hat{s}\cdot\vec{\beta}}. \tag{2.22}$$

With the obtained expression, a phase of the incident electromagnetic wave (Equation 2.21) can be transformed. When substituted into the equation for the scattered electric field (Equation 2.20), a dependence on the retarded time $t^{'}$ can be eliminated. In the resulting equation, there is a change in phase

$$E_s(R,t) = r_e\left[\frac{E_i}{\gamma(1-\beta_s)^3 R}((1-\beta i)(1-\beta_s) - \beta_e^2(1-cos\theta))\right] cos(k_s R - \omega_s t - \vec{k}\cdot\vec{r}_{p0}) \tag{2.23}$$

where k_s is the wave vector and ω_s is the angular frequency given by the following expressions:

$$k_s = k_i \left(\frac{1 - \beta_i}{1 - \beta_s} \right) \tag{2.24}$$

$$\vec{k} = \vec{k}_s - \vec{k}_i \tag{2.25}$$

$$\omega_s = \omega_i \left(\frac{1 - \beta_i}{1 - \beta_s} \right) \tag{2.26}$$

$$\omega = \omega_s - \omega_i = \vec{k} \cdot \vec{v} \tag{2.27}$$

As it was mentioned before, the change in frequency is due to the Doppler effect. From the last expression it can be seen that the Doppler shift is proportional to the component of the electron velocity $\vec{v}$ in the direction of vector $\vec{k}$.

2.5 The Salpeter parameter

In the previous parts, only the scattering on a single electron was considered. This section will also discuss more general conditions when this assumption is valid and when it is necessary to include the collective phenomena. In a volume containing N electrons, the resulting field is given by the sum of contributions from every single electron (Equation 2.23). However, only electrons with the same phase term $\vec{k} \cdot \vec{r}_{p0}$ (or 2π shifted) will contribute to the given direction. The so-called scale length is $2\pi/k$. The magnitude of the vector $\vec{k}$ can be written as ([9])

$$k = \frac{2\pi}{\lambda_i} sin \frac{\theta}{2}, \tag{2.28}$$

with the assumption that $\omega_s \approx \omega i$, where λ_i is the wavelength of the incident radiation. The assumption may not be valid with higher velocities, but the goal is to obtain only the idea about the scale of the scattering events. The Salpeter parameter α is introduced as the ratio of the scattering length and the Debye length λ_D:

$$\alpha = \frac{1}{k\lambda_D} = \frac{\lambda_i}{4\pi\lambda_D} \frac{1}{sin\frac{\theta}{2}}. \tag{2.29}$$

By the parameter α we can distinguish three different behaviour of the spectral distribution function. Scattering on just free electrons can be assumed if $\alpha \ll 1$. In this case, called incoherent scattering, the scattering length is much smaller than Debye length, which represents if the plasma evince collective behaviour, and electrons does not show any correlation between electron positions.

In the second case where $\alpha \geq 1$, also called coherent or collective scattering, scattering happens on electron inside of shielding clouds surrounding each ion in the plasma. Electrons follows the motion of the ion - their positions are correlated. Despite the fact that it is the electrons that scatter the light the electrons follows ions (their positions are correlated) and thus the diagnostic is more difficult. On the other hand it is one of the few ways how to gain information about the ions.

This can be useful especially for alpha particles as they can be source of the strong heating in the future fusion devices.

The last case where $\alpha \gg 1$ is also called coherent scattering. Collective electron movement can be seen and spectrum of electron density fluctuations can be determined.

The majority of Thomson Scattering diagnostics uses visible (ruby laser, $\lambda = 0.694\mu m$) or near infrared lasers (YAG laser, $\lambda = 1.06\mu m$) light source on scattering angles close to either 90 degree or 180 degree (LIDAR systems) in which case $\alpha \ll 1$.

2.6 Scattered spectrum

The final paragraph will be dedicated to the derivation of the scattered spectrum function S. This formula can be obtain from the expression for the average scattered power of group of electrons per unit solid angle $d\Omega_S$ per unit angular frequency $d\omega_S$. The derivation of the equation is similar as for the Equation 2.23 (proper procedure can be found in [9]). On top of that Fourier transformation is applied on the term $E_S(R,t)$ which leads to the $E_S(\omega_S)$. As a consequence of that Dirac delta function $\delta(\vec{k}\cdot\vec{v}-\omega)$ will appear as a transformation of exponential function in the final formula for the average scattered power:

$$\frac{d^2\vec{P}}{d\Omega_s d\omega_s} = r_e^2 \int_V \langle S_i \rangle n_e d^3\vec{r} \int_{vel} (\frac{\omega_s}{\omega_i})^2 \left[1 - \frac{\beta_e^2(1-cos\theta)}{(1-\beta_i)(1-\beta_s)}\right]^2 (1-\beta^2) f(\vec{\beta}) \delta(\vec{k}\cdot\vec{v}-\omega) d^3\vec{\beta} \tag{2.30}$$

In this equation $\langle S_i \rangle$ stands for time-averaged Poynting vector of incident wave, n_e is electron density and $f(\vec{\beta})$ is electron velocity distribution. Term $\frac{\omega_s}{\omega_i}$ is velocity independent thus can be taken out of integral. It represents blue shift of the spectrum. Term $(1-\beta^2)$ is responsible for decrease of scattered light intensity as a result of relativistic change of mass. Term $1 - \frac{\beta_e^2(1-cos\theta)}{(1-\beta_i)(1-\beta_s)}$ describes orientation change of the electric field intensity vector $\vec{E_i}$ from the perspective of moving electron. It can be demonstrated ([9]) that it has a small effect on the shape of scattered light spectrum but it has a negative impact on intensity.

Spectral function S is determinated by Equation 2.30. In the first approximation polarization can be set to unity. In majority current fusion devices depolarization term can be neglected since the its effect on intensity can be noticed at the higher temperatures only ($\geq$ 10 keV), see Figure 2.3b.

Lets suppose relativistic Maxwellian distribution function of the electron velocities:

$$f(\beta) = \frac{\alpha}{2\pi K_2(2\alpha)} \frac{e^{\frac{-2\alpha}{\sqrt{(1-\beta^2)}}}}{(1-\beta^2)^{\frac{5}{2}}} \tag{2.31}$$

where $\alpha = \frac{m_0 c^2}{2k_B T}$, K_2 is modified Bessel function of the second order and second kind, k_B is Boltzmann's constant and T is temperature [K]. The Equation 2.30 can be rewritten:

$$S = \int\int\int (\frac{\omega_S}{\omega_i})^2 (1-\beta^2) f(\vec{\beta}) \delta(\vec{k}\cdot\vec{v}-\omega) d^3\vec{\beta} \tag{2.32}$$

Detail derivation of the final equation can be found in [9]. Variables x and normalised wavelength shift ε, defined by the wavelength of incident λ_i and scattered λ_s wave, can be introduced:

$$\epsilon = \frac{\lambda_s - \lambda_i}{\lambda_i} \tag{2.33}$$

$$x = \sqrt{1 + \frac{\varepsilon^2}{2(1 - cos\theta)(1 + \varepsilon}} \tag{2.34}$$

Final analytical equation is:

$$S(\varepsilon, \theta, 2\alpha) = \frac{e^{-2\alpha x}}{2K_2(2\alpha)(1+\varepsilon)^3} \frac{1}{\sqrt{2(1 - cos\theta)(1+\varepsilon) + \varepsilon^2}} \tag{2.35}$$

Even with depolarization effect neglected, it has been shown [10] that this final analytical formula is reasonable accurate for high temperature plasma. Spectral function dependence on ϵ for different electron temperatures can be seen in Figure 2.3a. Relativistic blue shift effect on scattered spectra can be clearly seen even for 1 keV temperatures.

Final calculation can be performed without neglecting depolarization effect (as has been shown in [9, 5]). As a result correction factor q can be introduced. As can be seen in Figure 2.3b, it remains constant (which justificate neglection of depolarization effect) for the broad range of normalised wavelength shift ε values. On the other hand decrease of intensity for very high ($\geq$ 10 keV) plasma temperatures start to be appreciable. The depolarization effect has a maximum for the standard TS geometry ($\theta = 90°$.

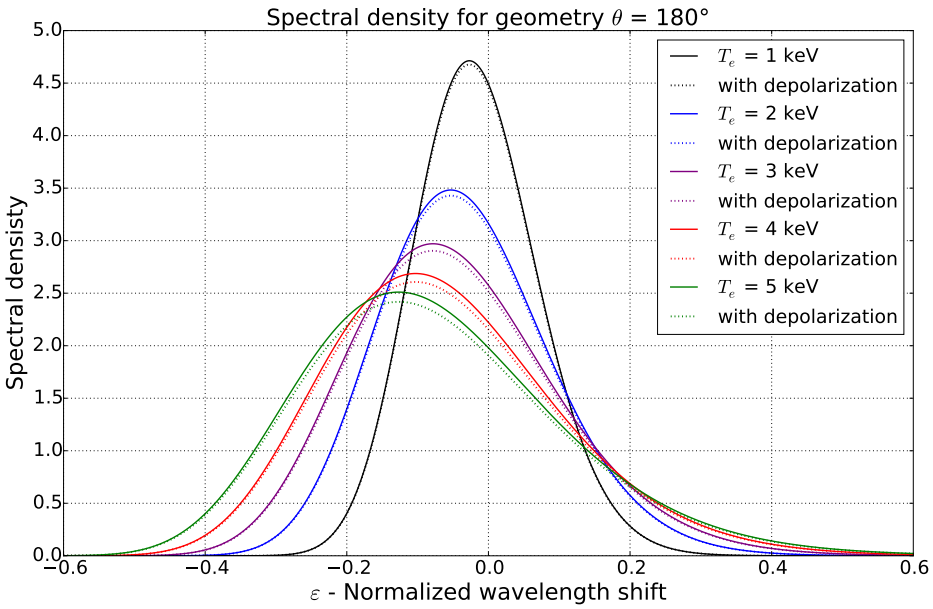

(a)

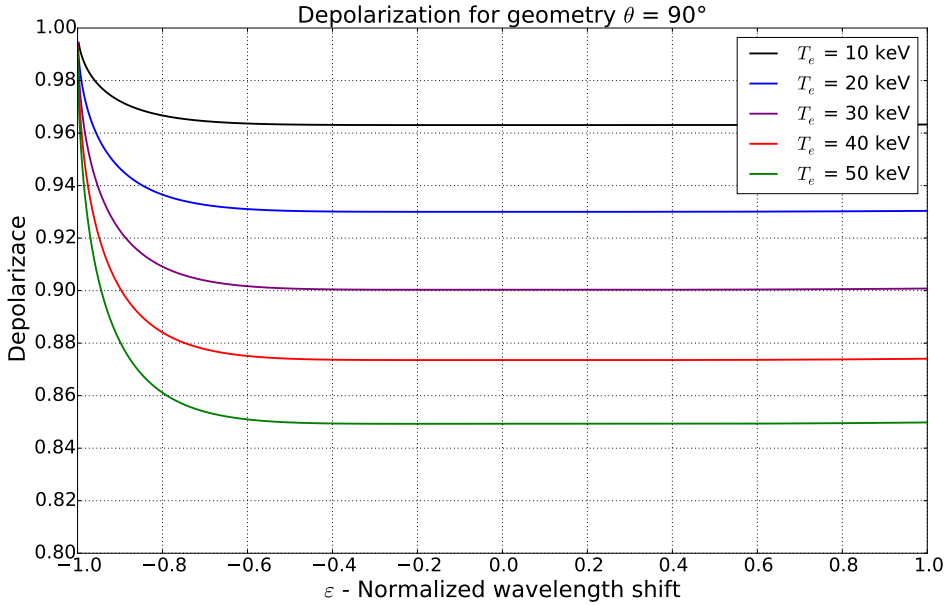

(b)

Figure 2.3: (a) Spectral density profiles and (b) depolarization correction factor as a functions of normalised wavelength shift ε for several temperatures. Courtesy: Miroslav Sos

3. Thomson Scattering on COMPASS

Broad variety of diagnostics were built in order to fulfil the scientific goal of the COMPASS tokamak ([12], Appendix I). The Thomson scattering (TS) diagnostic should contribute to it by providing temporally resolved electron temperature and density profiles with high spatial resolution and with focus to the plasma edge. With regard to absolute and self-reliant values of electron temperature, TS is considered to be one of the main diagnostics and reliable data are expected. TS diagnostic consists of the following subsystems:

- Laser system
- Laser transmission, injection optics
- Beam dump
- Collection optics
- Fibre-optic bundles
- Polychromators
- Control and data acquisition system

Specifications and parameters of the subsystems are given by requirements on the TS measurements, like spatial and temporal resolution and accuracy, and environment and conditions of TS operation, like available geometry for installation or background signal from the plasma.

3.1 Requirements

The most important requirement, given by the edge plasma region focused scientific program, was ability to see pedestal barrier. Pedestal parameters were, from Culham measurements [M.Valovic, IBA Meeting, Praha, 4 -5 April 2005, cited from Pedestal database H.Meyer 2004], predicted to vary in position from 0.71 m to 0.74 m and in width to vary from 0.01 to 0.02 m in R coordinate (see 3.1). These numbers, transformed for expected plasma configurations to vertical z axis, give estimated position in the range of 0.22-0.30 m above the centre of the vessel and width around 0.02 m. Basic requirements are ability to measure full profile with an adequate spatial resolution to be able to analyse pedestal (e.g. ability to derive pedestal position and width). In the same time, reasonable time resolution to cover different regimes of plasma discharge is needed. The range in which the diagnostic should provide the electron temperature and density data is 50-5000 eV for $n_e \geq 5 \cdot 10^{18}$ m^{-3}.

Apart of the pedestal region, the rest of the plasma should be covered with a lower resolution, reaching from centre on one side to the inner side of the pedestal region on the other.

Required maximal T_e measurement error is 10

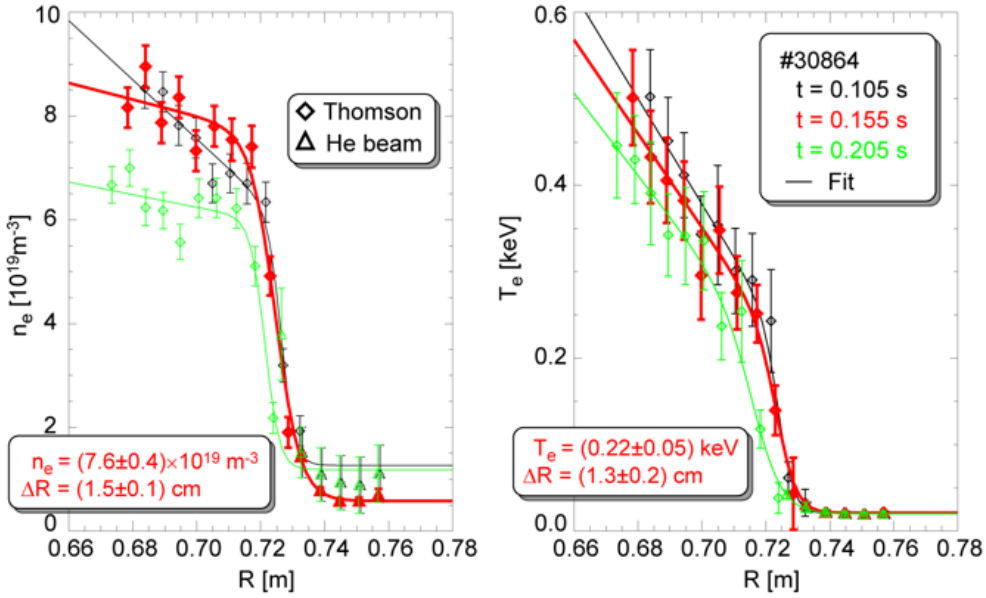

Figure 3.1: COMPASS-D measurements of pedestal, Culham, UK laboratory.

The TS system should provide measurements repetition rate of at least 30 Hz, covering all tokamak discharge duration. Option of a regime with two measurements separated by an arbitrary time delay was requested.

3.2 Constrains

3.2.1 Signal level

TS cross-section is very small and thus high power probing laser is needed. The TS phenomena gives for given geometry (solid angle and scattering angle, see Appendix II Section III) for the whole relevant spectral range approx. $10^3 - 10^4$ scattered photons per 1 cm of scattering length (i.e. corresponding to 1 cm spatial resolution) in the pedestal area. Signal is further reduced through the collection optics, optical fibres and spectrometer (polychromator). Calculations of the photon budget are presented in (Appendix III Section 4).

3.2.2 Bremsstrahlung plasma radiation

Background radiation plays an important role in the design of TS system, because it decreases signal to noise ratio. Bremsstrahlung as a part of this radiation can be calculated by [2]:

$$P_B \mathrm{d}\Omega \mathrm{d}\lambda_s = 2.09 \times 10^{-36} g Z^2 \left(\frac{n_e n_i}{\lambda_s^2 T_e^{1/2}}\right) \exp\left[-\left(\frac{1.24 \times 10^{-4}}{\lambda_s T_e}\right)\right] V_p \frac{\mathrm{d}\Omega}{4\pi} \mathrm{d}\lambda_s(W) \tag{3.1}$$

Where Z stands for charge of the ion, g is the Gaunt factor... Assuming the spectral bandwidths of the polychromators (as will be described further), 10 ns integration time, $Z = 2.5$, $n_e = 10^{19}$ m^{-3}, $T_e = 1$ keV and the geometry of the COMPASS TS system, number of Bremsstrahlung photoelectrons expected

in individual polychromator channels varies between 10 photons (for the narrow channel next to the laser line) and 300 photons (the widest channel).

3.2.3 Line radiation

An exact determination of line radiation intensities as another part of background radiation is quite a complex task. Collisional-radiative model should be used for correct calculations in tokamak plasma. In the first approximation, we assumed Boltzmann distribution for ions and we used weakly ionized plasma approximation given by the Saha equation between the ion stages to estimate the presence and the importance of the line radiation. Calculations were done using National Institute of Standards and Technology database for plasma composed of H and He with light (B, C, N, O) and heavy (Fe, Cr, Ni) impurity traces of 10^{-2} and 10^{-4} respectively. It was found that the most significant lines in the spectrum for TS based on ruby laser will be H I (656.3 nm), He I (541.1 nm), He I (587.6 nm), He I (667.8 nm), He I (706.5 nm), He I (728.1 nm), C IV (580.1 nm) and some additional lines for very high temperatures only. Based on the rough estimate from weakly ionized plasma COMPASS TS system will not be significantly influenced by line radiation since in the case of Nd:YAG laser, these lines are not in the measured spectral range.

3.3 Design

The above stated requirements and constraints resulted in a choice of TS system based on Nd:YAG lasers as a probing light source and filter polychromators with avalanche photodiode (APD) detectors for spectral characterisation of the scattered signal. The subsystems are briefly introduced here, with references to the papers with further details. Layout of the COMPASS cross-section with collection optics can be seen in 3.2

3.3.1 Laser System

To cover relatively short COMPASS plasma pulses, which vary in range of hundreds of millisecond up to one second, and in the same time supply sufficient energy for fine spatial resolution (down to 3 mm), solid-state lasers with Nd:YAG (neodymium-doped yttrium aluminium garnet) crystals and flash-lamp pumping were chosen. Two individual lasers allow their separate operation, for an arbitrary time delay between two adjacent TS measurements. Each laser has 1.5 J pulse energy, 30 Hz repetition rate and wavelength of 1064 nm. The laser systems is described in (Appendix III Section 2) and especially (Appendix IV), the safety system for lasers is presented in (Appendix V)

3.3.2 Laser transmission, injection optics and beam dump

The lasers are located outside the tokamak hall, the laser beam path from the laser output to the tokamak is about 20 m long. The beam is focused to the measurement region by a plano-convex lens. The beam enters the tokamak from a top

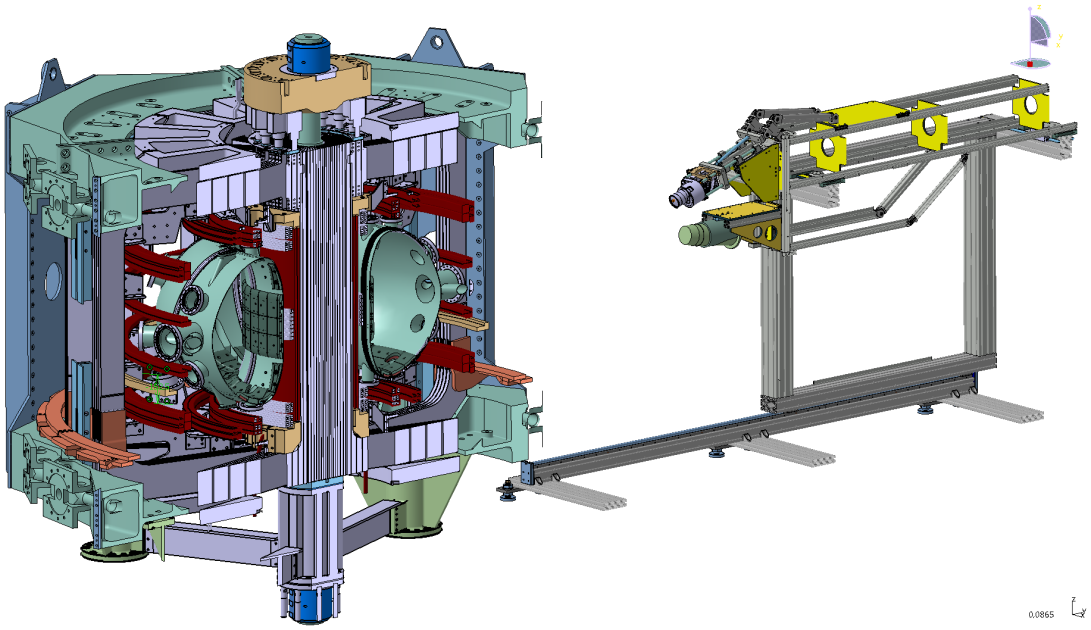

Figure 3.2: COMPASS cross-section with cut through trolley with Thomson scattering collection optics

through a Brewster vacuum window, which is followed by a pipe with two apertures stopping a stray light to enter the collection optics. After passing through the observed region (scattering region) in the plasma, the beam is terminated in a beam dump located below the tokamak inside a vacuum pipe extension. More details about the laser beam path and beam dump are in (Appendix IV).

3.3.3 Collection optics

The observed region is divided into two parts - core and edge. Each part is observed by an individual collection lens, optimised for required spatial resolution. The core lens observes plasma from -30 mm below tokamak midplane to 210 mm above midplane, with a spatial resolution of 10 mm in vertical direction. The edge lens overlaps with the core one at several spatial points, ranging from 195 mm to nearly 290 mm, with spatial resolution between 4 mm and 5 mm in the most spatial points and up to 6 mm in the furthest points. The edge lens design and installation was very challenging, because of the available geometry of the viewing ports on the tokamak. The design of both lenses is described in (Appendix II Section III), the core system commissioning in (Appendix VI) and commissioning of edge and more detail characterisation of both lenses in (Appendix VII).

3.3.4 Fibre-optic bundles

The collected light is transferred from the tokamak to the polychromators, which are located outside the tokamak hall because of easy access and electromagnetic interference, through optical fibres. The fibres are organised in bundles, each bundle being on spatial point when imaged to the plasma by the collection lenses. Every two fibre bundles are connected to one polychromator, the two corresponding spatial points are then resolved through fibre bundle length difference and

thus different scattered light pulse arrival time. This technique is called "duplexing" and saves number of polychromators. Details of optical fibre bundles are in (Appendix III).

3.3.5 Polychromators

The collected light is spectrally analysed in polychromators. The polychromator is a cascade of spectral filters, each of them passing through a selected band of wavelengths and reflecting the res to the next one. The transmitted light is then detected by a fast avalanche photodiode. Onboard electronics prepare the signal for digitisation. The details of polychromators and filter set design are in (Appendix II) and (Appendix III).

3.3.6 Control and data acquisition system

The electric signal from polychromators is digitised. Temporal evolution of the scattered signal is resolved with 1 GS/s digitiser with 120 channels. Slow data acquisition system is used for background light observation. The fast digitisers are controlled with a program written in LabView environment, the signals are further processed using a set of routines written in IDL programming language. Details of data acquisition are in (Appendix VIII).

3.3.7 Calibration

TS diagnostic is a complex diagnostic, including the required calibrations. Basically two calibrations are necessary - relative and absolute. Relative calibration is a spectral calibration and is necessary namely for resolving electron temperature, i.e. reconstruction of the scattering spectra. The absolute calibration relates total strength of the scattered signal with electron density measurements. Raman or Rayleigh scattering on the gas of known pressure is used for this purpose around the world, on COMPASS Raman is used. Both calibration techniques are presented in (Appendix II). A spatial calibration relates the measured data to the plasma (Appendix VII).

3.4 Measurements and results

The commissioning of the system and first data is in (Appendix VI), the error analysis and some plasma parameters derived from TS measurement are (Appendix IX), another error analysis is in (Appendix X), edge TS system first measurements are in (Appendix VII). Measurements of T_e, comparing data from probes and TS, are in (Appendix XI). Analysis of quasicoherent modes in the tokamak, using also TS data, is presented in (Appendix XII). A description of H-mode plasma in the COMPASS tokamak, including the profiles obtained by TS, is in (Appendix XIII).

3.5 Instrument function

Instrument function is describing the TS system characteristic in space, its ability to resolve some spatial structures. At first sight, spatial resolution is given by location of each spatial point and its length. This would be true in 1D, when the laser beam is of zero diameter. But since the laser beam cross section is finite and it is observed along a viewing chord of finite cross section and in non-perpendicular direction, the instrument function may not be so trivial. For the below presented calculations, a beam of Gaussian profile was assumed. The model was simplified by introducing 2D projection in a plane given by the laser beam and viewing chord. The laser beam was then summed over the dimension perpendicular to this plane, making it 2D. A viewing chord for each spatial chord was then simulated, taking into account the viewing chord size as obtained by imaging the spatial fibres through collection lens, and scattering angle from the spatial calibrations. To relate the measurements to the tokamak radius coordinate, i.e. onto the mid-plane, which is generally used by other diagnostics, magnetic reconstruction of magnetic surfaces was used. It is presumed the plasma properties, like temperature and density, are constant along the magnetic surface, which can link any point on the vertical axis to the mid-plane. Magnetic configuration from selected tokamak shot number and time is presented in 3.3. The region of scattering is illustrated by blue colour, the mid-plane region is illustrated by dark red.

Examples of results, for selected spatial points from both core and edge TS systems, are shown in 3.4, 3.5 and 3.6. The lines represent the calculated instrument function for individual spatial points. The filled rectangles give comparison with the simple "1D model" mentioned above. As can be seen, the difference is not so significant mostly. But e.g. in 3.4 there is a difference. This can be explained by proximity of the plasma centre, the curvature of magnetic surfaces passing through the scattering region is high.

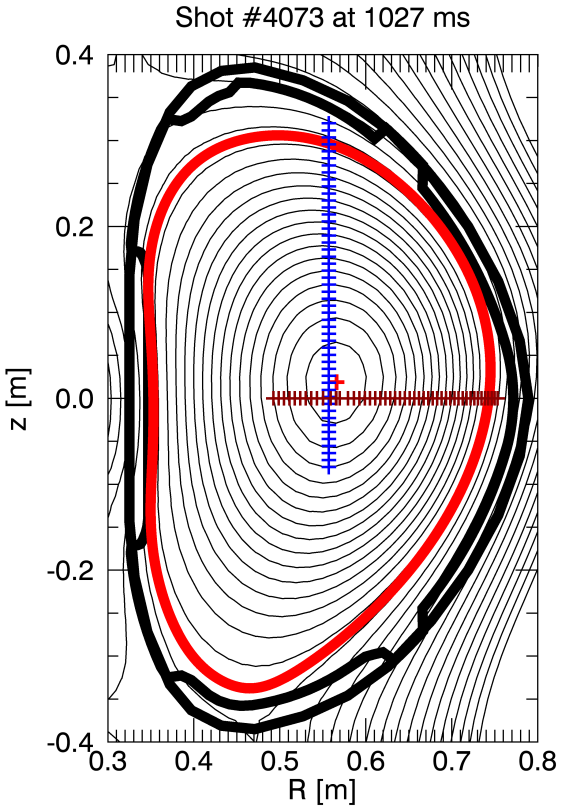

Figure 3.3: Magnetic surfaces reconstruction (from EFIT code) of the COMPASS tokamak plasma cross section, as was used for relating TS data measured along the vertical axis (blue) with mid-plane axis (dark red).

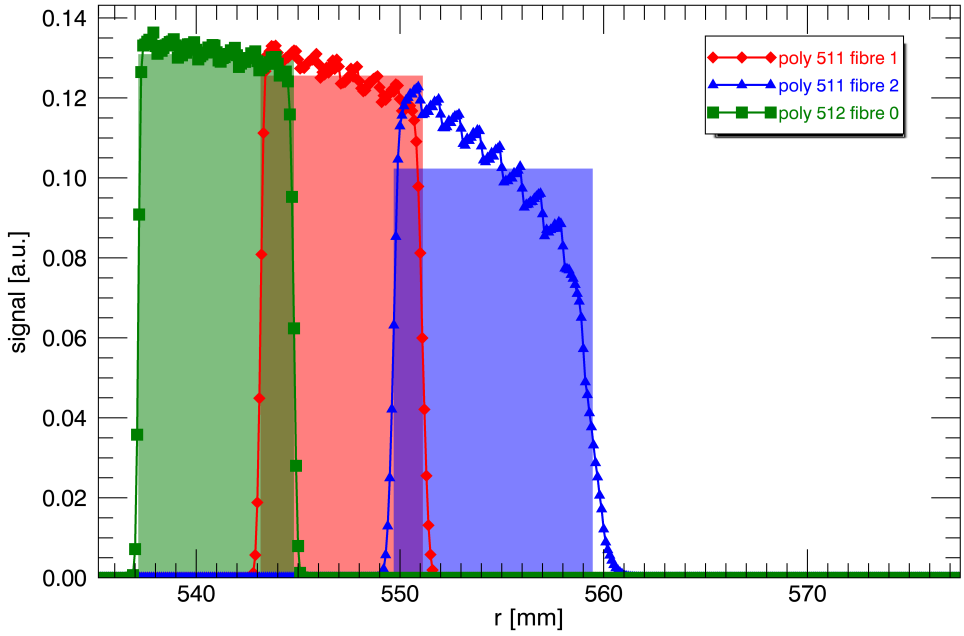

Figure 3.4: Example of instrument function of several core TS spatial points close to the plasma core.

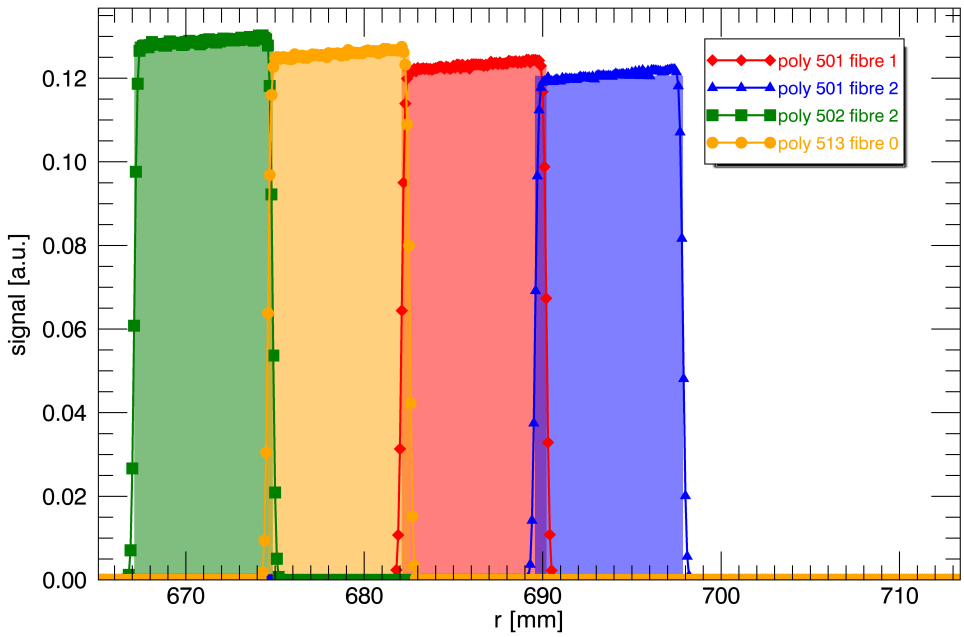

Figure 3.5: Example of instrument function of several spatial points from outer part of the core TS view.

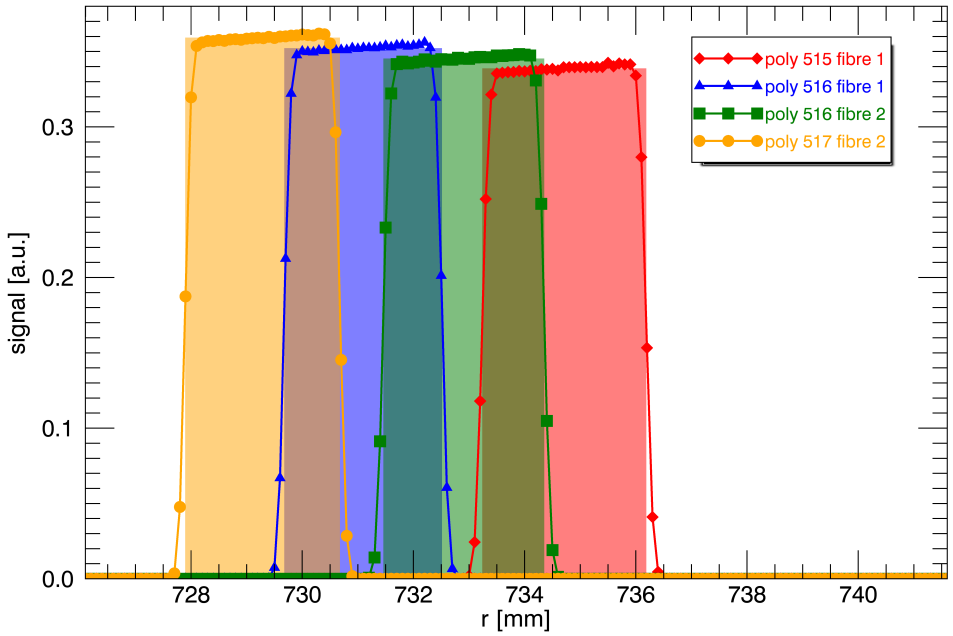

Figure 3.6: Example of instrument function of several edge TS spatial points.

4. ITER

ITER is an international tokamak aimed make use of the studies of high temperature plasma physics and move the knowledge of plasma physics and material science further toward a nuclear fusion reactor and demonstrate feasibility of production fusion power electricity on Earth (Figure 4.1; parameters summarized in Table 4.1). ITER is being currently build in south of France, close to Cadarache research centre . It is a common project of European Union, India, Japan, China, Russia, South Korea and the United States. The facility construction is expected to be finish in 2019. The year after, 2020, will start the first plasma experiments. Full deuterium-tritium fusion experiments are expected to start in 2027.

Total Fusion Power	500 MW
Q – fusion power/additional power	≥ 10
Average 14 MeV neutron wall loading	0.57 MW/m^2
Plasma inductive burn time	≥ 400 s
Plasma major radius (R)	6.2 m
Plasma minor radius (a)	2.0 m
Plasma current (Ip)	15 MA
Vertical elongation @95% flux surface/separatrix (κ_{95})	1.70/1.85
Triangularity @95% flux surface/separatrix (δ_{95})	0.33/0.49
Safety factor @95% flux surface (q_{95})	3.0
Toroidal field @6.2 m radius (B_T)	5.3 T
Plasma volume	837 m^3
Plasma surface	678 m^2
Installed auxiliary heating/current drive power	73 MW
Additional Heating and Current Drive - Total injected power (Electron Cyclotron, Ion Cyclotron, lower Hybrid, Negative Ion neutral Beam)	Up to 110 MW

Table 4.1: Summary of ITER parameters [1]

The most parts of the ITER (coils, diagnostics, heating systems, etc.) are built according to the ITER design as in-kind contributions of the partner organizations (Domestic Agencies) which handle and guarantee the delivery. The European Domestic Agency is Fusion for Energy (F4E). The system how the Domestic Agencies design and build the mentioned parts of ITER consist of several steps:

1. Determination of which Domestic Agency is responsible for which parts (e.g. edge Thomson scattering diagnostic system was assigned to Japan Atomic Energy Agency (JAEA), Domestic Agency of Japan; core Thomson scattering diagnostic system has been assigned to Europe, F4E)

2. ITER specifies what requires and demonstrates feasibility of fulfilling these (demanding) requirements. This can be described as:

   (a) ITER (possibly in collaboration with Domestic Agency) creates design

   (b) ITER organizes Design Review (DR). During this review the design is presented to panel of experts from all over the word (from the field and

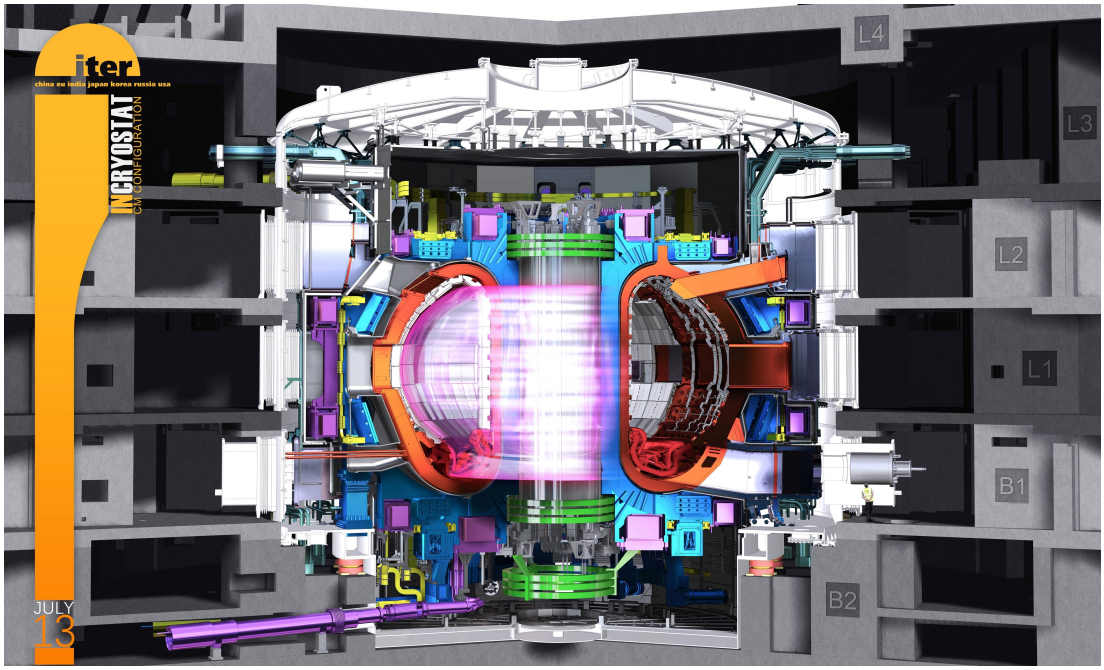

Figure 4.1: Tokamak ITER overview with plasma. Image credit: ITER Organization

fields which the design interfaces to) together with representatives of ITER and responsible Domestic Agency. Purpose of DR is to review the design and address its flaws and weaknesses with a main goal to judge feasibility of the design with the current technology (and possibly advise further steps and improvements; requirements can be also disputed).

3. If the feasibility of the design is approved, Domestic Agency is authorized to deliver the object of the design (While all specified requirements are mandatory, alternation of the design is allowed)

4.1 Work for ITER

As the COMPASS TS team (P. Bilkova, P. Bohm, M. Aftanas), we have been invited to help with two separate TS systems for ITER – Edge Thomson scattering system and later on also Core Thomson scattering system. For these two systems we have been working on the design, aiming to fulfil the given requirements and to prepare the Design Report (for Design Review). This work has been organized by M. Bassan (ITER organization) and in case of Edge TS system we have been collaborating with Japan Domestic Agency (JAEA - T. Hatae, E. Yatsuka).

My part mostly covered data acquisition, signal and background estimation, error estimation, calibration and alignment. I participated also in both DR and presented part of the design to the panel of experts. In the following sections, the design of the two mentioned Thomson scattering systems will be described.

4.2 Edge Thomson Scattering System

The Edge Thomson scattering system (edge TS) will provide the electron temperature and density profiles for physics studies and advanced plasma control. Real-time reliable profiles of Te and ne are required since the diagnostic will be used for advanced machine control. Next role of the edge TS is understanding the H-mode, indication of the L-H transition, and ELM physics (see Table 4.2).

Measurement	14. H-mode: ELMs and L-H transition indicator	14. H-mode: ELMs and L-H transition indicator	23. Electron temperature profile	24. Electron density profile
Parameter	ELM density transient	ELM temperature transient	Edge T_e	Edge n_e
Measurement Role	Physics	Physics	Physics	Advanced Control
Contribution	Supplementary	Supplementary	Sole primary	Primary
Condition	r/a>0.85	r/a>0.85	r/a>0.85	r/a>0.85
Range	$5 \cdot 10^{18} - 3 \cdot 10^{20}$ m^{-3}	0.05 - 10 keV	0.05 - 10 keV	$5 \cdot 10^{18} - 3 \cdot 10^{20}$ m^{-3}
Time resolution	10 ms	10 ms	10 ms	10 ms
Spatial Resolution	5 mm	5 mm	5 mm	5 mm
Accuracy	5%	10%	10%, $n_e > 2 \cdot 10^{19}$, 20%, $n_e > 5 \cdot 10^{18}$	5% $n_e > 2 \cdot 10^{19}$, 10%, $n_e > 5 \cdot 10^{18}$

Table 4.2: Summarised measurement specifications and contributions of the edge Thomson scattering system.

4.2.1 Requirements

The important requirements given by the role of the diagnostic are:

- time resolution 10 msec, assuming scaling of pedestal parameters with a^2, and extrapolating from JET data
- spatial resolution 5 mm for $r/a > 0.85$ but the consequences of failing to meet this requirement are less severe the further into the plasma the pedestal reaches
- maximum value of the error in n_e measurements is 5 % in the range $2x10^{19} - 3x10^{20}\ m^{-3}$ but could be 10 % in the range $5x10^{18} - 2x10^{19}\ m^{-3}$ without operational issues.

For the edge TS system as all TS systems density and temperature errors are linked through photon statistics. Thus, a 10 % error for densities in the range

$5x10^{18}$-$2x10^{19}$ m^{-3} corresponds to a 20 % statistical error for temperature. This means that the ITER requirements (10 ms / 10% on the T_e edge measurement) will only be met by the edge TS for the innermost part (typically 80 %) of the edge profile. For quasi-static conditions this will not be an issue, as averaging several laser pulses and compensating for edge movement with magnetics will allow 10 % or lower errors on a 50 ms time-scale. Faster events can be investigated by using the slow evolution of the edge TS profiles to calibrate the response of the backup system, X-ray crystal spectrometer (survey and edge high resolution). This will come at the expense of effective edge resolution however.

With regard to the edge transient parameters for ELMs, needing a time resolution of 0.1 ms, 3 modes of operation could be considered to satisfy this supplementary role:

Mode 1 A 'passive' way, by statistical analysis of edge profiles, correlating them off-line with time markers of the ELM evolution provided by reflectometry, spectroscopy and ECE.

Mode 2 Dedicated operation could be considered, synchronizing some laser shots with ELM pre-triggers. A pre-trigger must be available at least 300-350$\sim \mu$s in advance, due to the time needed for build-up of the population inversion in the YAG lasers. This would require some ability to vary the laser dwell time, from 10 ms to an upper limit determined by the need to keep laser operation stable. However, this option is in conflict with the beam combination technique using a scanning mirror.

Mode 3 Provide a real-time evolution of a specific ELM profile. An array of several lasers would be needed, or even several lasers able to operate in burst mode. This option has not been considered further in this conceptual design since it would add another complexity to the design and could decrease reliability the the system to fulfil primary role of the diagnostic.

In summary, the specification adopts a time resolution of 10 ms for this function, in Mode 1, with Mode 2 to be considered as part of the detailed design.

4.2.2 Challenges of ITER edge TS

The implementation of the Thomson scattering for ITER edge TS system poses a number of challenges. For the system front end, specifically the collection optics and embedded beam dump, challenges include:

- Thermal survival range 300–525 K (625 K for plasma facing components)
- Exposure to large neutron fluxes and associated effects
- Strong thermal gradients and associated effects
- Severe EM loads from disruption events
- Potential mirror coating and erosion
- Very limited space to install instruments

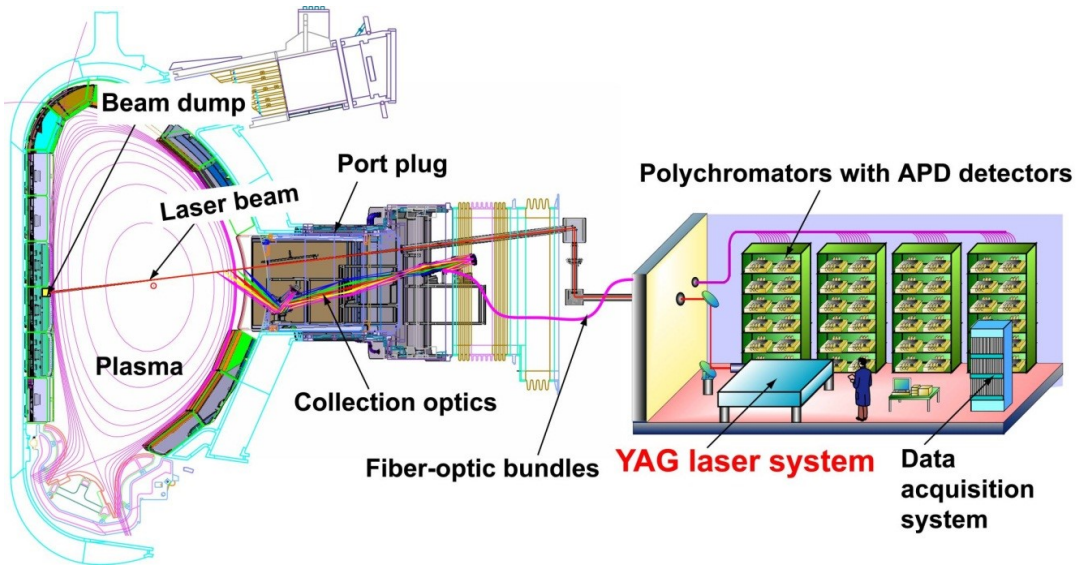

Figure 4.2: Basic concept of the edge Thomson scattering system. Image credit: ITER Organization

- Maintaining viewing field alignment with tight space requirements

For intermediate part of the system, specifically laser transmission & injection optics, and fibre-optic bundles challenges include:

- Exposure to large neutron fluxes and associated effects at system front end
- Exposure to high energy density of laser beam
- Maintaining high precision alignment in real time
- Maintaining beam quality on the long beam path

For the system back end, specifically the laser system challenges include:

- Development of high-energy and high-repetition laser to satisfy measurement requirements

4.2.3 Design

The edge Thomson scattering system is composed of following sub-systems as shown in Figure 4.2:

1. Laser system
2. Laser transmission, injection optics
3. Beam dump
4. Collection optics
5. Fibre-optic bundles
6. Polychromators

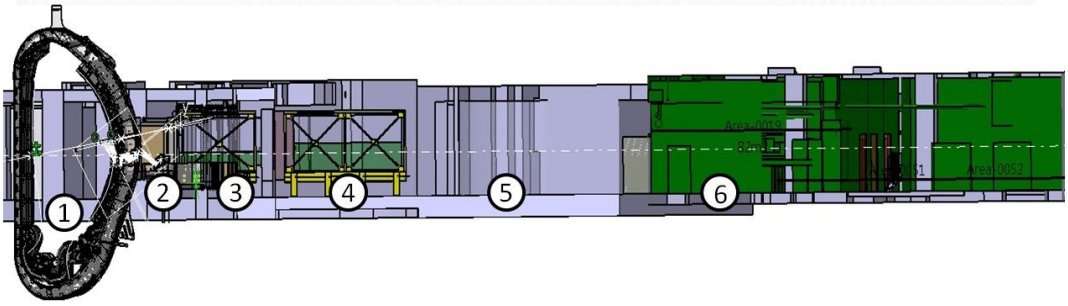

Figure 4.3: Distribution of Thomson scattering component in the ITER tokamak complex. 1) Plasma chamber; 2) Port Plug; 3) Interspace; 4) Port Cell; 5) Gallery; 6) Cell in Diagnostic Hall. Bio-shield is between 3 and 4. The second confinement wall/barrier is between 4 and 5. Image credit: ITER Organization

7. Control and data acquisition system

The edge Thomson scattering system is a distributed system with components throughout the ITER tokamak complex. The collection optics will be installed in the peripheral vertical drawer of the Equatorial port #10 module. A part of collection optics (fibre coupling optics, fibre plug holder) will be installed in the port cell. A beam dump will be installed near the vacuum vessel boundary, and embedded in the blanket module #4. Laser transmission and injection optics and fibre-optic bundles will be installed between the interspace and the Diagnostic Hall, especially the laser injection optics will be installed in the port cell. The laser system, polychromators with APD detectors, control and data acquisition system will be installed in one of the cells of the Diagnostic Hall (see Figure 4.3).

Space has been allocated in the peripheral drawer 1 of Equatorial port 10 (EP10) for the edge TS. The port plug, port cell and interspace region are shared with the core Thomson scattering system and the poloidal polarimeter.

4.2.4 Laser system

In order to satisfy the temporal resolution of 10 ms, a Nd:YAG laser (YAG laser) system is the best solution, and YAG lasers are widely used in recent Thomson scattering systems (Compass , DIII-D, JT-60U, JET, MAST, NSTX). In order satisfy the required accuracy, laser with 5 J at 100 Hz are needed. In any case for general reliability reasons of the diagnostic at least 2 independent lasers will be needed for edge TS. The performance of nowadays commercially available lasers with respect to repetition rate and energy is substantially lower than the ITER target.

Japan Domestic Agency have developed a prototype YAG laser system (Figure 4.4) for the edge Thomson scattering system in the ITER by applying the basic laser design used for the JT-60U system that addresses the high-energy/high-frequency limits correcting the beam quality by phase conjugate mirrors.

4.2.5 Beam dump

A beam dump is used for the purpose of safely terminating the laser beam and minimizing the generation of stray light. The beam dump will be installed at

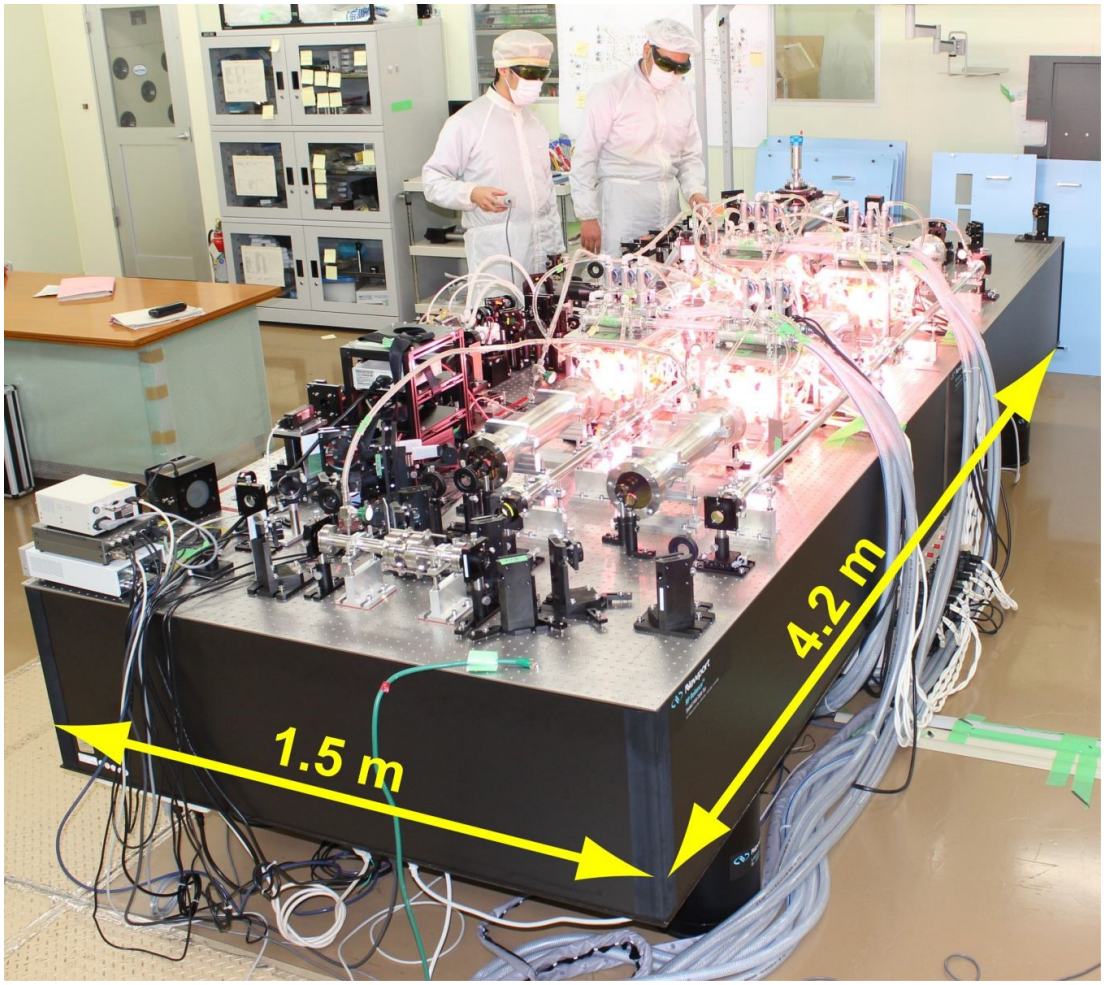

Figure 4.4: Picture of prototype YAG laser system. Image credit: Japan Domestic Agency

a blanket module in the vacuum vessel. In the design of the beam dump, it is necessary to fulfil as many as possible simultaneously of often mutually conflicting conditions as summarized in table Table 4.4.

From the viewpoint of reduction of stray light, reflectivity of beam dump material is as low as possible because of absorption of the laser power. A larger beam dump size and a smaller beam diameter are most favourable for effective reduction of stray light. Considering the installation into a blanket module, smaller size of the beam dump is required. For steady-state heat load derived from nuclear heating and radiation heating, a smaller size and material with high thermal conductivity are needed to cool the beam dump. In the case of the instantaneous heat load generated by the laser pulse, the influence of extremely high energy density must be considered: high reflectivity material is preferred to avoid the laser damage; large aperture is necessary to decrease the energy density; high thermal conductivity material is necessary for cooling. Considering of the skin effect, low electrical conductivity is also needed to obtain long skin depth. In order to survive from disruption event, it is necessary to minimize the electromagnetic force, so a small beam dump is desirable, and low electrical conductivity is also desirable to minimize the eddy currents.

A chevron type (Figure 4.5 (d)) adopting the beneficial features of both type

Function	Reflectivity	Size	Thermal conductivity	Electrical conductivity	Entrance beam diameter
To reduce stray light	Low	Large			Small
To allow installation into BSM		Small			Small
To reduce steady-state heat load (nuclear heat and radiation heat-derived)		Small	High		Large
To reduce instantaneous heat load (laser-derived)	High	Large	High	Low	Large
To reduce electromagnetic force (by disruption)		Small		Low	
To monitor and control beam positionl	High				Small

Table 4.3: Beam dump parameters and their desirable characteristic for each function

using plane parallel plates has been proposed. In the chevron type, the plates are inclined to avoid facing the plasma directly, and multiple reflections are possible in a limited space. The following shape parameters characterize the optical performance:

- Thickness of chevron plate
- Space between chevron plates
- Number of bends
- Bends angle

Japanese Domestic Agency performed analysis with these effects taken into account:

- polarization of laser beam
- thermal analysis - radiation and neutral particles
- laser induced damage threshold
- electromagnetic forces

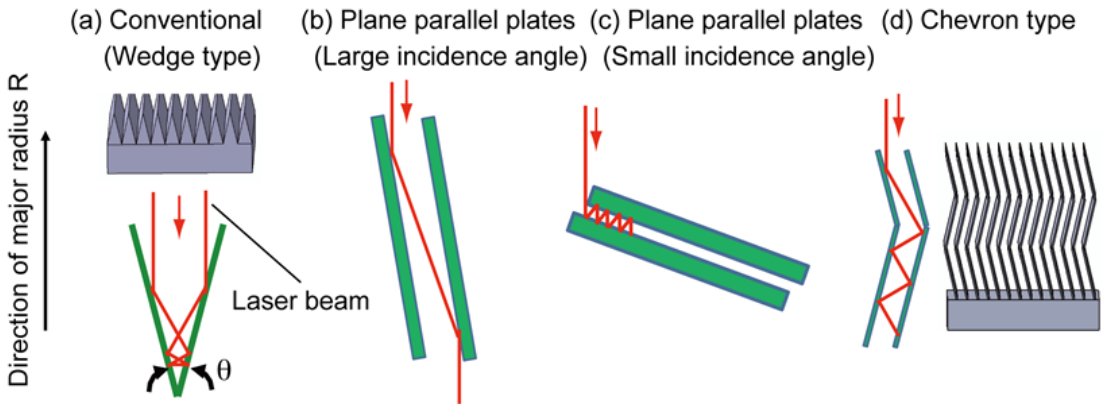

Figure 4.5: Alternative shapes of beam dumps.

- raytracing of returning light

of all Chevron plate variables, the resulting optimised beam dump design is summarized in Table 4.4.

Parameter	Value
Thickness of chevron plate	1 mm
Spacing of plates	2 mm
Number of bends	3
Bending angles	18°,14°,20°
Polarization state	s
Material	Molybdenum

Table 4.4: Optimized parameters for beam dump

4.2.6 Optics

The system proposed for the Edge TS system (Figure 4.6) consists of a mirror optical system in the Port Plug and a hybrid mirror and refracting system for the optical path in the Interspace area which forms a final image approximately 2 m from the Closure Plate of the Port Plug. Optics performance summary can be seen in Table 4.5.

4.2.7 Fibre optics

Following parameters has been taken into account and simulated/calculated to find optimal design:

- Radiation Resistivity. Defects can be partially heal by heat-treatment ([6])
- Resistance to heat load
- Maximization of the signal
- Misalignment effects

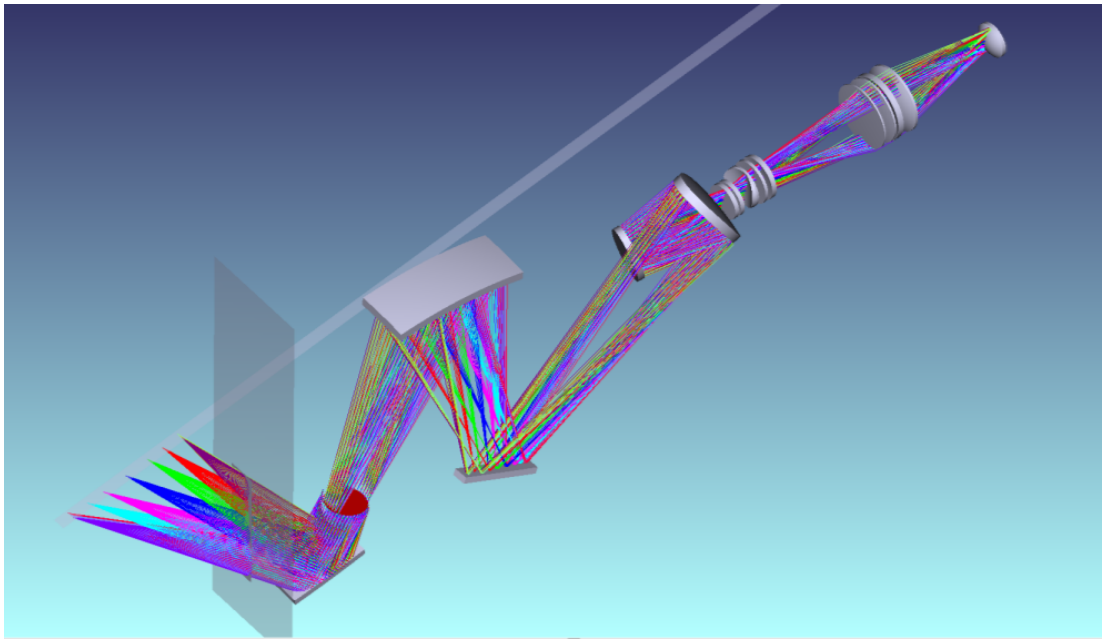

Figure 4.6: Complete Optical system

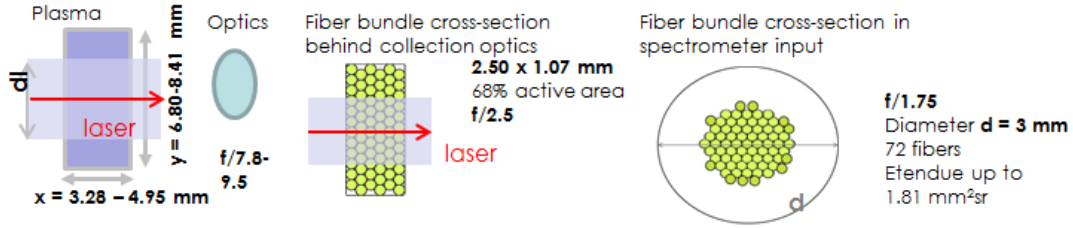

Figure 4.7: Details of the light collection geometry

The fibres holder will be motorized in order to compensate for the slow movements of the mirrors with the port plug, mostly related with the changes in the operating temperature. Fibre bundles are going to be 40-50 meters long. Material of fibre was chosen so that fibres can survive exposure to radiation. There will be no more than 10 μSv/hour in the area starting 0.5 m behind closure place. Total expected neutron fluency during the shot will be 108 n/cm^2 but only a small fraction of them (2.5 %) are high speed neutrons. Therefore (10^{-1} to 10^{-2}) dB/m attenuation of fibres at the end of ITER life time is estimated. In front of the bundle a high efficiency polarizer will be added to reject 50 % of the plasma light and improve the S/N ratio.

4.2.8 Polychromators

Suitable polychromators have already been developed (DIII-D, MAST) and are in use on existing machines and hence developments from scratch of new designs and technology are not required. Measurement up to an electron temperature of 10keV requires measurement down to at least ~700 nm, preferably to ~600 nm at a scattering angle of 150 degrees.

The detected pulse duration should be as short as possible to ensure the minimum background light is included in the signal. Further to this, as the beam

Field of View	570 mm
Object Space Aperture Ratio	F/8.5
Image Space Aperture Ratio	F/2.7
Wavelength Range	530 - 1100 nm
Magnification	x0.32
Encircled Energy	90% in 1.24 mm diameter spot at image (3.88 mm diameter at laser)
Footprint at Vacuum Windows	Within 150 mm diameter
Vacuum Window Position	At Closure Plate
Surfaces	Spherical plus one Cylindrical Corrector Plate
Lens Materials	F-Silica and radiation hardened LF5G15

Table 4.5: Optics performance summary

dump is 3.5 m from the scattering volume, light reflected from the beam dump will reach the lens ∼21 ns after the scattered pulse. For this reason the convolution of laser pulse duration, APD detector response and amplifier response must be significantly less than 21 ns. The combined detector and amplifier impulse response should be shorter than the laser pulse duration.

The detected scattered signals are fast pulses of order 10-20 ns. The error on the measured scattered pulses is set not only by the shot noise on the scattered pulse but also by the magnitude of slow varying background light. For the purposes of digitisation however there are limited bits available for fast digitisers (recently up to 10-12 in the 1 GS/s range) hence it is convenient to separate out fast and slow outputs. Filtering signals below 100 kHz removes slow varying background light, this background light output should be separately digitised by a slow sampling ADC. Hence the polychromator should produce a fast as well as slow output.

In a cascaded optical filter polychromator design, spectral channels will see a number of reflections and transmissions dependent on their position within the spectrometer. Typical losses on lens transmission are of order 0.3 % and losses on mirror reflection are of order 0.5 % for a di-electric mirror. The peak optical transmission of an interference filter is typically > 85 %, but can be higher for broader filters. The reflectivity of the filter outside of the pass-band is > 99 %. Hence, even for a 7 channel cascade the losses on lenses and mirrors are not dominant. For this reason the polychromator layout should be optimised for ease of manufacture and set-up and not simply to minimise optical losses on components.

Another important aspect to consider is blocking of the laser light. Blocking at the laser wavelength of 10^{-5} can be achieved by interference filters. As an empirical result a blocking of this magnitude works on typical experiments where efforts are made to minimise stray laser light.

The size of wavelength bands of spectral channels as a function of wavelength should be sufficiently narrow to diagnose Te at that wavelength. Additional considerations are that wavelength bands near the laser wavelength should be de-

signed to measure Raman signals in at least one, preferably two spectral channels, and that the H_α line must be avoided.

The Figure 4.8 shows a typical spectral band configuration and wavelengths required to measure up to various temperatures. Measuring down to a wavelength of 700 nm nearly fulfils the 10 keV requirement, however a lower wavelength channel ensures good measurements at this temperature.

The Figure 4.9 shows the filter transmission bands required to measure nitrogen (here at $T_{gas} = 300$ K, the channels would similarly work at $T_{gas} = 400$ K). One advantage of the layout shown here is that the Nitrogen spectrum is divided evenly between two spectral bins hence each polychromator provides two independent measurements of the density calibration for that spatial point. The important requirement is that the filter transmission bands should be sufficiently close to the laser wavelength to allow Raman calibration.

4.2.9 Control and Data Acquisition System

Depending on the number of polychromators (e.g. 120) and number of spectral channels (6-7, assume 6 on average) it is necessary to synchronously digitize approximately 720 spectral channels. Each spectral channel has two outputs – one with low-pass filter and one with high-pass filter. This approach allows measuring the fast photodiode signals on a smaller signal range (from the high-pass filter side) thanks to the subtraction of background radiation and improving the resolution.

Requirements:

- Automatic synchronized data acquisition with correct timing with respect to given trigger sequence.
- Identification of which laser has triggered the data segment.
- Configuration of all ADCs to follow different ITER operation regimes

The high-pass filter outputs of the polychromators need fast digitizers. Bandwidth is determined by the laser pulse waveform and response time of the polychromator avalanche photodiodes and circuit. An analog bandwidth > 100 MHz is required for amplification of laser pulse width < 12 ns. Sampling rate is required to be > 1 GSample/s. Bit resolution is derived from possible signal and background noise range.

The bremsstrahlung radiation has been estimated as approximately $2{\cdot}10^{17} \sim$ photons $\cdot m^{-2}{\cdot}sr^{-1}{\cdot}nm^{-1}{\cdot}s^{-1}$ flat across the whole wavelength area, which gives us (for scattering area cross section = 5x5 mm^2; F# = 8.9; etendue $25x10^{-8}$ $m^2{\cdot}sr$; acquisition time 12 ns) 600 photons$\cdot nm^{-1}$.

For the widest spectral channels these assumptions mean a signal background fluctuation of up to 10,000 photoelectrons, in the same order of magnitude of the signal (up to 40,000 photoelectrons for 4th channel and up to 20,000 photoelectrons for the others). At least 10 bit resolution (1024 logical levels) is needed to adequately digitize the signal. Low-pass filter output can be digitized with slower digitizers with higher resolution (at least 100 kSample/sec, 16 bit). Control and DAQ system should be equipped with embedded computers to provide fast pre-processing of the TS data in the cabinets.

Correct calculation of the electron density from the TS signals needs information about incident light intensity. Laser energy for each pulse will be measured from the partially transmitted light by one of the mirrors. This light will be homogenized in an integration sphere, then the signal recorded with a fast photodiode and digitized with one additional fast ADC channel. Amplitude and evolution of the signal will be compared with a calibrated laser shot.

4.2.10 Supplementary Systems

Laser beam alignment has to be monitored remotely through fast cameras (≥ 100 Hz in order to catch all laser pulses) on each mirror in all areas with limited access (gallery, port cell, bio-shield, interspace area, port-plug) and on the vacuum window. Controllers for motorized mirror mounts have to be installed for all mirrors that need to be remotely controlled.

Stability of the mirrors has to be monitored: a diode laser will be mounted on each mirror or pointed to the mirror, and the projected/reflected laser beam spot will be detected by additional cameras ($\sim$Mpx resolution). Surfaces of mirrors, lenses and windows have to be also controlled by high resolution ($\sim$Mpx) cameras (with controlled RGB LEDs illumination) at normal/slow speed for off-line assessment of the surface quality and by fast PIN diodes for detection of enhanced diffuse laser light, an indication of possible surface damage. Temperature value and gradient of mirrors in port plug will be monitored with thermocouples (2 for each mirror plus 2 extra for the one closest to the plasma).

4.2.11 Calibration

Absolute calibration TS systems have two options for independent absolute calibration: Rayleigh or Raman scattering from an in vessel gas. Both calibration techniques have been shown to work on existing systems. In particular for polychromator based TS systems NSTX and DIII-D have successfully calibrated from Rayleigh scattering. COMPASS, JET, MAST and RFX have calibrated from Raman scattering in Nitrogen. Either technique can be used, but Raman scattering has a number of advantages in that it uses existing Thomson scattering filters and does not require neutral density filters.

Raman Scattering: Polarisation Scattered signals from Raman scattering are divided in the ratio 4:3 in polarisations parallel to and orthogonal to the laser wavelength respectively. It is assumed for this analysis that the collection optics transmission is completely independent of polarisation of scattered light. A polarizer in any case is installed in front of the optical fibres for rejection of the plasma light.

Raman Scattering: Gas choice Hydrogen and Deuterium most useful lines are above the scattering laser wavelength which does not fit well for Raman scattering calibration. Scattering from Nitrogen provides a useful spectrum in the range 1045-1064 nm for a 1064 nm laser and so is the obvious gas choice. It is estimated for an F/9 system with a 5 mm scattering length a 2.5 J laser will

produce ∼100 detected photoelectrons from Raman scattering in Nitrogen. Calibration for a pressure range of approximately 10-100 mbar will provide adequate signals, although calibration on MAST using averaging has been done for down to 0.1 mbar. This equates to a much (x10 or more) higher pressure for Hydrogen or Deuterium, unfeasible also for safety reasons considering the large volume of the vacuum vessel (800 m^3).

Figure 4.10 shows the scattered signals from the 3 gases at room temperatures. The most intense lines for hydrogenic gases are above the laser wavelength as these are the transitions dependent on the population of $n = 0$ and $n = 1$ levels. The width of the Raman spectra increases with increasing gas temperature.

Raman Scattering: Spectrum shape, T_{gas} The gas pressure and temperature in the vessel must be measured, both of which have uncertainty. Since the Nitrogen Raman spectrum shape is gas temperature dependent, if the signal is measured in two spectral channels this can either be used as an independent measurement of absolute calibration co-efficients or as a measure of vessel temperature.

Spectral Calibration The minimum wavelength to be measured is set by the highest electron temperature to be measured. Measuring to 800 nm will diagnose temperatures up to 3 keV. Measuring to 680 nm is close to but marginal for 10 keV. Measuring to 550 nm will very easily diagnose 10 keV. These requirements are illustrated by example in Figure 4.11.

First mirror The first mirror of the system is likely to be Molybdenum and is likely to show significant variation in spectral transmission across the range of required TS measurements. Possibly a layer of Rhodium will be used to coat Mo and improve the performances. It is not known how quickly these variations will occur, that is whether the spectral response will vary significantly after 103, 104 or 105 seconds of plasma operation and hence a variety of different spectral calibration monitoring techniques will be required.

Raman Lines from Multiple Lasers Raman lines from multiple lasers from either purely Nitrogen or Nitrogen and a Hydrogenic gas provides an option for a 'two point' or 'three point' spectral calibration but not detailed transmission measurements. This requires injection of a known transmitted energy of a different laser.

The Figure 4.12 shows the wavelength spread achievable for scattering from a variety of gases and lasers. This technique would provide calibration at a number of distinct wavelengths but would leave large gaps in the spectrum also.

Dual Laser Calibration If two or more lasers are used for Thomson scattering measurements this provides a basis for spectral calibration. There are multiple ways to envisage this calibration. For example if the two spectra do no overlap and spectral calibration has been performed using a white light source then using the two lasers for independent TS measurements simply provides an independent check, similar to using ECE to compare against TS measurements.

If the scattered signals from the two lasers overlap, then the ratio of the scattered signals in a spectral channel centred at $\sqrt{\lambda_1 \lambda_2}$ is independent of electron temperature. The relative magnitude of scattered signals in this bin provides the ratio of laser energy measurement. The signals in other channels from the two lasers can either be used to find electron temperature independently of transmission or to estimate the transmission and a temperature.

The Figure 4.13 shows the spectral range overlap achieved using different combinations of scattering lasers. A 532 nm laser will not provide a good wavelength overlap for expected temperature and so is not a useful calibrating laser. A 694.3 nm laser will provide independent measurements of TS spectra in the lower wavelength channels. At 2-3 keV the ruby laser will provide useful calibration measurements up to 1000 nm. The least practical laser option, 800 nm, would potentially provide very useful calibration of the primary laser system even at relatively low temperature.

In-vessel light source An in-vessel light source moved via remote handling can be used to back illuminate the TS light collection with a source of known emissivity and hence provide a spectral calibration. The disadvantage of this technique is that on ITER the calibration intervals will be in the order of years.

Back Illumination A reflective surface can be installed on the back of the shutter protecting the edge TS collection mirror. One of the TS optical fibres or a dedicated fibre can then be back illuminated with a source of known emissivity located in the Polychromator room and reflected light monitored from the other fibres. The light from this source will be diffused from the back of the shutter and hence will see every element in the optical path twice except the reflector which it will see once. This technique will need an intense light source and some modelling to ensure light back reflected from one optical fibre will close to fully fill the etendue from adjacent fibres.

An alternative to using a white light source for this technique is to use a pulsed light source, such as an OPO laser source or Ultrabright SLS [8]. A pulsed light source has the advantage that it can provide measurements with fine spectral resolution measurements, and the much higher intensity than a conventional source.

Calibration Optical Fibre There may be a change in transmission as a function of wavelength due to the optical fibre irradiation and or darkening due to neutron flux. It would be useful to separate out loss of transmission due to optical fibres from that due to the collection lens system. One convenient way to estimate this is have a single calibration optical fibre which is twice the length of TS optical fibres. This calibration fibre would follow the path of the TS fibres but double back on itself at the fibre tray, both ends of this fibre being located in the polychromator room. The transmission of this optical fibre could be measured directly in the polychromator room.

Alternative Path Calibration An alternative narrow light path penetration designed into the port plug can allow a bypass light source which can illuminate the rear of the shutter directly. In this case, metal mirrors can be used

as these are not subject to any degradation by main plasma or glow-cleaning systems. This will provide a robust means of calibration of all the mirrors.

Spectral Calibration Strategy The spectral calibration will likely prove more difficult than absolute calibration and is also more difficult than spectral calibration of the divertor Thomson scattering due to the range of wavelength that needs to be covered. The best approach to spectral calibration is to use as many of the above techniques as possible:

1. Pulse to pulse monitoring:
    - Dual Laser Calibration
    - Comparison with ECE
2. Frequent periodic measurement:
    - Back illumination. The use of dedicated fibres will allow calibration even after every ITER shot.
3. In-frequent measurements (once a campaign):
    - Raman from multiple lasers
    - Illumination from an in vessel source

4.2.12 System Performance - Simulation results

Parameters used for the performance simulations are:

- 5 J laser pulse energy
- Laser transmission losses (20 coated window/glass surfaces + 12 mirrors): 20 %
- Collection optics transmission (including losses in fibers and filling ratio): 10 %
- 12 ns measurement time
- Bremmstrahlung contribution: $2.0 \cdot 10^{17}$ photons$\cdot$s$^{-1}\cdot$m$^{-2}\cdot$sr$^{-1}\cdot$nm^{-1}
- High efficiency polarizer
- quantum efficiency: 80 %
- APD noise factor: 4

Results (Figure 4.14) are consistent with the requirements.

4.3 Core Thomson Scattering System

Core Thomson Scattering system (Core TS) is required to contribute for advanced machine control and physics studies, and has supplementary role only for basic machine control or protection. The implementation of the core Thomson scattering system on ITER poses a number of challenges. For the system front end, specifically the collection optics and embedded beam dump, challenges include:

- Thermal survival range 300 – 525 K (625 K for plasma facing components)
- Exposure to large neutron and γ-rays fluxes and associated effects
- Strong thermal gradients and associated effects
- Severe EM loads from disruption events
- Potential mirror coating and erosion
- Very limited space to install instruments
- Maintaining viewing field alignment with tight space requirements

For intermediate part of the system, specifically laser transmission and injection optics, and fibre-optic bundles challenges include:

- Exposure to large neutron and γ-rays fluxes and associated effects at system front end
- Exposure to high energy density of laser beam
- Maintaining high precision alignment in real time
- Maintaining beam quality on the long beam path

For the system back end, the challenges include:

- Development of high-energy and high-repetition laser system to satisfy measurement requirements
- Development of high speed ADCs to measure the scattered light pulse and clearly identify and discard background plasma-light and laser stray-light.

4.3.1 Design

The Core TS is a distributed system with components throughout the ITER tokamak complex (Figure 4.15). A beam dump will be installed near the vacuum vessel boundary, and embedded in the blanket module #3. The collection optics will be installed in the peripheral vertical drawer #3 of the Equatorial port #10. A part of collection optics (fibre coupling optics, fibre plug holder) will be installed in the port interspace. Laser transmission and injection optics and fibre-optic bundles will be installed between the interspace and the Diagnostic Hall, in particular the laser focusing optics will be installed in the port interspace. The laser system, polychromators with APD detectors, control and data acquisition system will be installed in a dedicated room of the Diagnostic Hall.

Space has been allocated in the peripheral drawer 3 of Equatorial port 10 for the Core TS. The port plug, port cell and interspace region are shared with the Edge Thomson scattering system and the Poloidal Polarimeter. Space has been allocated in the blanket module (#3) for the beam dump. Space has been allocated in the diagnostic hall for the lasers and other back-end equipment. Access to the polychromators cabinets is possible without interfering with the lasers area. In consideration of the very limited maintenance foreseen for the spectrometers and of their relatively low power consumption, we plan to use cabinets up to 3 m tall for their installation. In the gallery and port cell behind EP10 space has been allocated for the laser transmission optics and fibre-optic bundles.

4.3.2 Requirements

Measurement	**Parameter**	**Contribution**	**Condi-tion**	**Range**
04. Plasma Energy	β_p	Supplementary	$r/a < 0.85$ $I_p > 3$ MA	0.01 – 5
06. Line-averaged electron density	$\frac{\int n_e dl}{\int dl}$	Supplementary	$r/a < 0.85$	$1 \cdot 10^{18} - 4 \cdot 10^{20}$ m^{-3}
23. Electron temperature profile	Core T_e	Primary	$r/a < 0.85$	0.5 - 40 keV
24. Electron density profile	Edge n_e	Primary	$r/a < 0.85$	$3 \cdot 10^{19} - 3 \cdot 10^{20}$ m^{-3}

Measurement	**Resolution**		**Latency**	**Accuracy**
	Time	**Space**		
04. Plasma Energy	0.1 ms	Integral		5 %
06. Line-averaged electron density	1 ms	integral		1 %
23. Electron temperature profile	10 ms	Req.: 67 mm Target: 50 mm	2.5 ms	10 %
24. Electron density profile	10 ms	Req.: 67 mm Target: 50 mm	2.5 ms	5 %

Table 4.6: ITER Core Thomson scattering requirements

The most stringent requirements are:

- 5 % accuracy in n_e measurements and 10 % accuracy in T_e measurements over the entire range $3 \cdot 10^{19} - 3 \cdot 10^{20}$ m^{-3}
- and 67 mm (target 50 mm) space resolution for $r/a < 0.85$

For quasi-static conditions this will not be an issue, as averaging several laser pulses and compensating for plasma movement with magnetics will allow 10 % or lower errors on a 50 ms time-scale. Faster events can be investigated by using the slow evolution of the Core TS profiles to calibrate the response of the ECE and of the backup system (X-ray crystal spectrometer). This will come at the expense of effective resolution.

With regard to the supplementary role for plasma energy and line-integrated density measurements, there is no possible mode of operation that can satisfy the time resolution of 0.1-1 ms, particularly on a continuous basis. The Core TS can only be used for cross-calibration.

4.3.3 Laser System

- Beam energy effectively injected in the plasma: 5 J
- Laser pulses repetition rate: 100 Hz
- Laser pulses duration full width (99 %): <12 nsec

A specific choice is not suggested, because of evolution of current technology. In principle the Pockels cell method is the most flexible, if issues of size, degradation with time and attenuation will be solved or significantly improved. Existing technologies can solve the propagation of the beam with the necessary low attenuation and directional precision.

4.3.4 Beam dump

Due to the size and location, the main task for the beam dump in ITER is not of preventing the generation of stray-light, but mainly of protecting the walls of ITER, avoiding drilling a hole in the wall and sputtering high-Z material into the plasma. Work is in progress for the improvement of the design and for the assessment of the long-term resistance of the device.

4.3.5 Collection Optics

The Core TS is a challenging diagnostic to design because it requires a large entrance pupil diameter to maximise the collection of scattered spectral emissions from the laser line plus a resolution requirement of R/30 (67 mm). The large entrance pupil diameter means the optical path in the diagnostic shield module is more difficult to fold for good neutron shielding. This necessitates a longer optical path length which in turn increases the difficulty of imaging the entrance pupil within the 160mm diameter of the Vacuum Windows.

The key features of created reference Zemax design:

- a large first collection mirror
- two in-port fused silica lenses, allowing to squeeze the light beams into the maximum allowance of the 160 mm diameter double vacuum window

- a complex lens assembly in the interspace area, to compensate for the large aberrations generated by the large angles of incidence on the collection mirrors
- attachment of the interspace optics directly onto the port-plug back-plate , in order to simplify the alignment when the internal collection optics moves with the vessel
- a complex focal surface, shaped in 3-D, for the correct assembly of the fibre optic head

The fibres holder will be motorized in order to compensate for the movements of the mirrors within the port plug, related with the changes in the operating temperature and with forces driven by the electro-magnetic fields. Piezo-driven motors are envisaged.

Note: During DR, there have been pointed out improvements which could increase performance of the system. Real optics for the Edge TS system can be significantly altered.

4.3.6 Fibre-optic bundles

The key issues are:

- 40-50 meter length
- careful shielding is needed to avoid transmission degradation in the DD and DT phases of ITER
- polyimide buffer to allow annealing up to a relatively high temperature

4.3.7 Polychromator

Polychromators with optical filters as opposed to 'CCD and diffraction grating' based spectrometers are the best candidate for diagnosing the spectrum of scattered light from the ITER core TS system.

The key issues are:

- 7-8 spectral channels
- Dedicated filters to reject the dominant H and H lines (and others possibly)
- Etendue > 2.02 mm^{2}sr
- Optimize integration with electronics

4.3.8 Control and data acquisition system

Control and data acquisition system has to satisfy three main tasks:

- scattering measurement
  - start, stop and manage measurements

Spectral filter	$\Delta\lambda$	N_{TS}	$?_{N_{fe^i}}$	N_{bg}
1	55	480	111	1273
2	55	936	136	2285
3	112	3066	251	10307
4	86	2975	196	5349
5	29	1020	125	1681
6	52	1911	156	3032
7	71	3582	203	5656
8	128	4144	924	171660

Table 4.7: Detected photoelectrons within 40 keV plasma (and with density of $3 \cdot 10^{19}$ m^{-3}). Actual values will depend on the laser energy and on the transmission (see paragraph 'Simulations')

  - measurement integrity verification

- configuration & calibration
- troubleshooting
  - fault recovery
  - test and conditioning

Assuming that a suitable high-pass filter will be adopted before the ADC, only the statistical noise is added to the fast TS signal. From Table 4.7 the S/N ratio is approximately 10, therefore the dynamic range of the ADC will not be significantly affected. Assuming a gain of 30, and a density of $3{\cdot}10^{20}$, a full-scale of approx. 10^6 electrons is expected, before the amplifiers. Considering a balanced transmission line of 100 ohm, and a pulse-length of 10 ns, the equivalent average input voltage before the amplifiers stages is 1.6 mV. Suitable amplifiers gain will be needed to match the full scale input of the selected ADCs.

High speed ADCs modules, using several interleaved ADC chips, that can reach 3-4 Gs/s and 12 bit resolution are available on the market but have several drawbacks for a system that requires approximately 500 fast channels:

- Low density of 2 channels/PXI slot: 250 slots
- High power consumption of 10 W/ch.: 5 kW for the ADCs only
- High cost, currently almost 10 kEuro/Ch: 2.5 MEuro for the ADCs only, assuming a 50 % reduction in the future

Instead Switched Capacitor Array (SCA) is proposed. The concept of a temporary ultra-fast analogue buffer integrated with a slower (and high precision) ADC is particularly suitable for a diagnostic like TS, that captures data with a very low duty cycle, of the order of 10^{-5}. The only drawback of the SCA technique is the finite and relatively short length of the buffer. However with the current devices featuring at least 1000 cells/channel, and a sampling rate of 5 Gs/s, the buffer can cover 200 ns: enough for at least 4 scattering measures, i.e.

the system will be suitable also for operation of the diagnostic in burst mode, if needed. Additionally future versions are expected to provide even longer buffers. The cost of commercial SCA-based ADCs is today about 20 times lower than for the traditional fast ADCs, the density is also more than 10 times higher, and the power consumption is 10 times lower.

Development of a dedicated and completely integrated board, including filters, amplifiers, SCA, ADC for both fast and slow sampling, for each spectrometer is suggested.

Summary:

- fast DAQ channels = 8×70×2 channels; ≥4 Gs/s; ≥10 bit, ≥200 MHz bandwidth
- slow DAQ channels = 560 channels; ∼100 kSample/s; ≥14 bit
- CPUs and lookup tables-based fast pre-processing

4.3.9 Calibration

This system is very sensitive to spectral transmissivity of optical components (collection optics, fibre-optic bundles) and spectral sensitivity of the detector. The design of CPTS has been carried out based on an assumption that the spectral transmissivity and sensitivity are fully calibrated. A set of verification-compensation systems for the spectral (and absolute) calibration are also part of the design, that can be used on a daily basis, or more frequently if needed:

- Compensation with reference fibre
- First mirror illumination with narrow spectrum diffuse light
- Multicolour scattering

Several calibration systems shall be needed to confirm the relative and absolute calibrations of the TS measurements. It shall be noted that it shall be possible and appropriate to use simultaneously more than one calibration method, in order to cross-check their results.

Spectral calibration of core TS is challenging, the available methods have to exploited in combination.

- short-term ('shot-to-shot')
  - multicolour scattering
  - cross-calibration with ECE diagnostic
  - reference fibre
- mid-term
  - first mirror illumination (possibly after each plasma shot)
- long-term
  - Raman from multiple laser wavelengths
  - polychromator calibration with white light source and monochromator
  - illumination from in-vessel source

4.3.10 Simulations

Background plasma light The background light generated by the divertor and collected by the optics has been estimated considering both the continuum emission and the line emission. Starting from the classic formula for the plasma emissivity:

$$\epsilon_\lambda = 9.45 \cdot 10^{-20} \cdot g_{ff}(\lambda) \cdot {n_e}^2 \cdot Z_{eff} \cdot \frac{e^{\frac{-1.24 \cdot 10^3}{\lambda \cdot T_e}}}{\lambda \sqrt{T_e}} \quad photon \cdot s^{-1} \cdot m^{-3} \cdot nm^{-1} \quad (4.1)$$

and modelling the divertor with:

- major radius $R = 5.0$ m
- minor radius $a = 0.3$ m
- volume $V = \pi a^2 \cdot 2\pi R = 8.9$ m3

Considering the dependence at 1000 nm of the emissivity on the divertor plasma temperature (Figure 4.16), the peak value has been selected. From that value and averaging it over the vessel area, and the resulting brightness value is:

$$B_\lambda = 1.3 \cdot 10^{17}\, photon \cdot s^{-1} \cdot m^{-3} \cdot sr^{-1} \cdot nm^{-1} \quad (4.2)$$

The line emission particularly from the boundaries has been estimated for different plasma scenarios. Then the ray-tracing program LightTools has been used to compare the amount of light collected by an observer in the position of the first mirror for both continuum and line emissions, as shown in Figure 4.17 and Table 4.8.

It is clear that unless the line emission is carefully avoided or filtered out, it can dominate the spectral channel background.

The dispersion of the TS signal in the i-th channel of spectrometers $\sigma_{N_{fe^i}}$ has been computed as follows:

$$\sigma_{N_{fe^i}} = \sqrt{k(N_{fe^i} + N_{bg^i}) + 2N_{AMP}^2} \quad (4.3)$$

where k is APD access noise factor, N_{bg} is number of photoelectrons related to background light, N_{AMP} is detector and amplifier noise reduced to the input of the detector (the values $N_{amp} = 50$ photoelectrons and $k = 2.44$ that coincides with an APD magnification coefficient equal to 30 have been used).

The spectral performances of each group of components has been used (Table 4.9). Almost all components (except A/R coating surfaces) shows almost constant behaviour in the range of 1100-500 nm with the fast drop to almost 0 % transmissivity between 500 and 400 nm range. Complete convolution gives total transmission of the collection optics of approximately 25-40

The performances and variances are reported for a T_e of 40 keV in Table 4.11.

For the simulation, channels 5 and 6 were merged, assuming that a notch filter can be used to reject the H_α. The total transmission has been halved to take into account aging of first mirror and other optics. The energy of the laser was taken as 4 J. It is quite evident that in order to be confident to obtain reliable measurements according to the requirements in actual operating conditions, with

species	Wavelength [nm]	Power [W] #2226	Power [W] #2436	Power [W] #2447
Be I	457.3	31701	30708	9905
Be II	467.4	0	0	0
He II	468.6	2531	2441	2798
He I	471.4	5527	931	225
Be II	482.9	0	0	0
D	486	38263	15454	4790
He I	492.3	8848	2342	540
He I	501.7	4166	1313	288
He I	504.9	643	154	36
Be II	527.2	0	0	0
He I	587.7	187108	40776	10631
D	656.1	151407	64397	26136
He I	668	30669	7953	1751
Ne	694.1	0	0	0
He I	706.7	31543	3581	970
Be I	721	3615	18425	7569
He I	728.3	2857	467	109
Be I	825.6	3667	4943	1710
D	874.9	238	96	22
D	886.1	312	126	29
D	901.3	422	170	39
D	922.7	592	237	54
D	954.4	868	347	80

Table 4.8: Total line emission power from the divertor and scrape off layer for three cases, and its wavelength and the species

A/R surfaces	N	32
bare surcafes	N	2
fibers	m	40
UV fused silica	mm	361
LF5G15	mm	56.5
LF5G19	mm	0
Dielectric Mirrors	N	4
Protected Ag	N	1
Molybdenum	N	1
Fibre fill ratio	%	69

Table 4.9: Optical elements used to compute the total transmission of the system (only peak values are mentioned here, but wavelength dependent values has been used)

Position ID	1
r/a	-0.102
L, scattering length [mm]	74
θ, scattering angle, [deg]	160.48
aperture of collection optics object F#	16.88
Image F#	2.64
Ω, field angle [sr]	$2.75{\cdot}10^{-3}$
Detected volume width [mm]	26.7
Etendue [m^2sr]	$1.278{\cdot}10^{-6}$
Laser pulse integration time [ns]	5
Plasma density [m^{-3}]	$3.0{\cdot}10^{-19}$

Table 4.10: Common parameters used in the simulations

Spectral filter	$\Delta\lambda$	N_{TS}	$\sigma_{N_{fe^i}}$	N_{bg}
1	55	715.6341	108.3152	1.02E+03
2	55	$1.34{\cdot}10^3$	129.9	$1.76{\cdot}10^3$
3	112	$4.19{\cdot}10^3$	228.9	$7.61{\cdot}10^3$
4	86	$3.86{\cdot}10^3$	180.7	$3.73{\cdot}10^3$
5	29	$1.36{\cdot}10^3$	119.2	$1.21{\cdot}10^3$
6	52	$2.72{\cdot}10^3$	151.5	$2.32{\cdot}10^3$
7	71	$4.29{\cdot}10^3$	182.4	$3.64{\cdot}10^3$
8	128	$4.66{\cdot}10^3$	714.3	$1.01{\cdot}10^5$

Table 4.11: Example of signals and variances at 40 keV

collection mirrors and/or fibre bundles partially obfuscated, it is appropriate to use a laser that can deliver a pulse of 4-5 J. The results are therefore consistent with the requirements only marginally in the region 30-40 keV: the 10 % limit on δT_e is only achieved in the best situation. The blue region will be the first affected by mirrors and fibres damaging, easily up to 600-650 nm. This factor was not included in the previous simulations. It will make the situation for 30-40 keV even worse, as made clear by the spectra in Figure 4.19, where the use of a ND:YAG laser at 1320 nm is also introduced.

The error curves computed for the 1320 nm laser show that in similar conditions, even with an enhanced background, it can provide significantly better performances than 1064 nm laser of the same energy in the region 5-40 keV. It can be concluded that the proposed design is able to meet the requirements in the first phases of operation of ITER, with maximum temperatures up to approximately 25 keV, and that with the only upgrade with a 1320 nm laser the measurement range can be extended up to 40 keV.

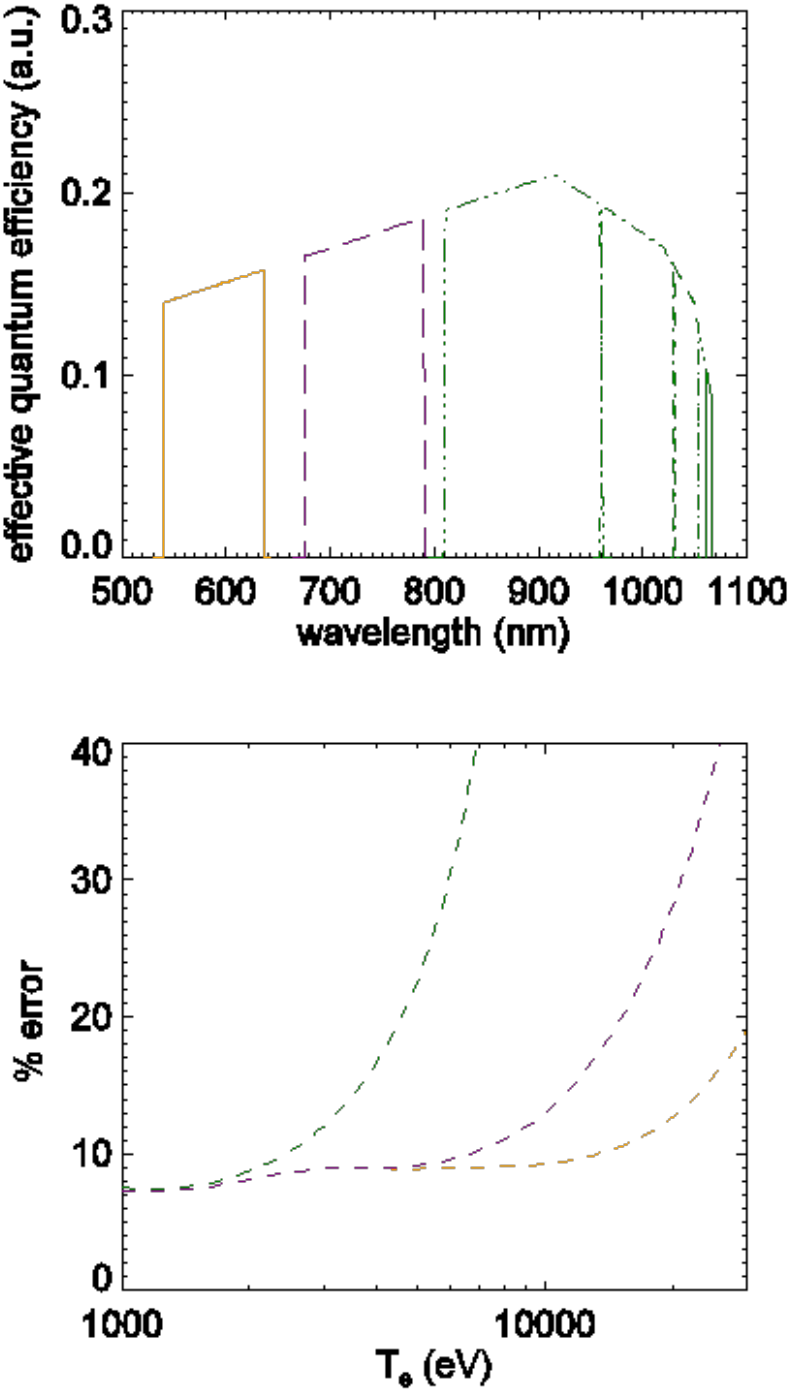

Figure 4.8: Potential spectral transmission bands and the fractional error on temperature resulting from the addition of various channels.

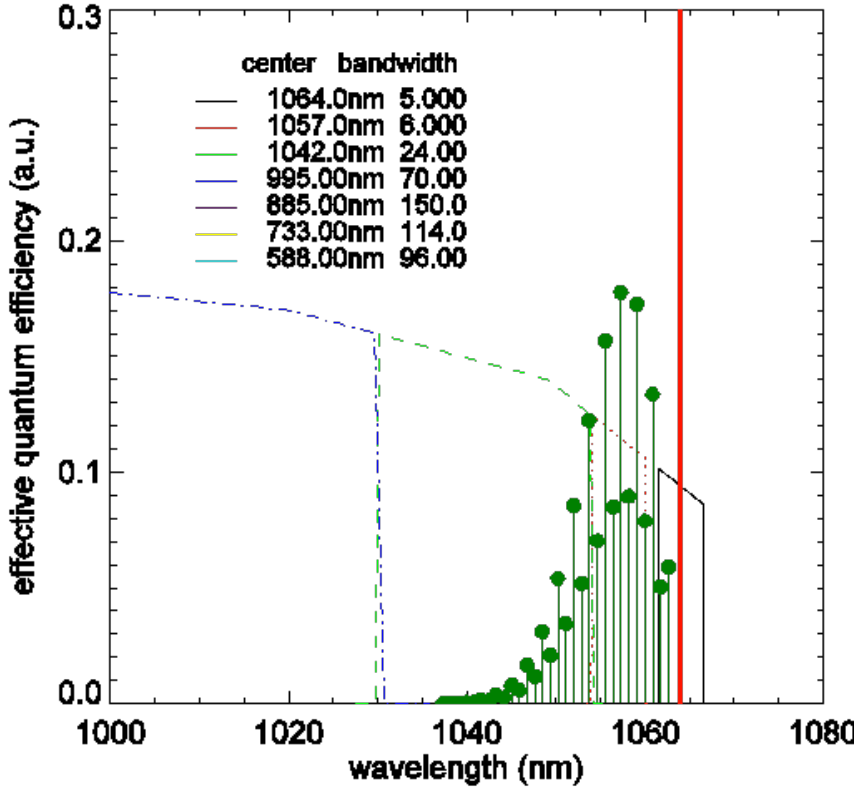

Figure 4.9: Raman scattered lines from Nitrogen gas at room temperature

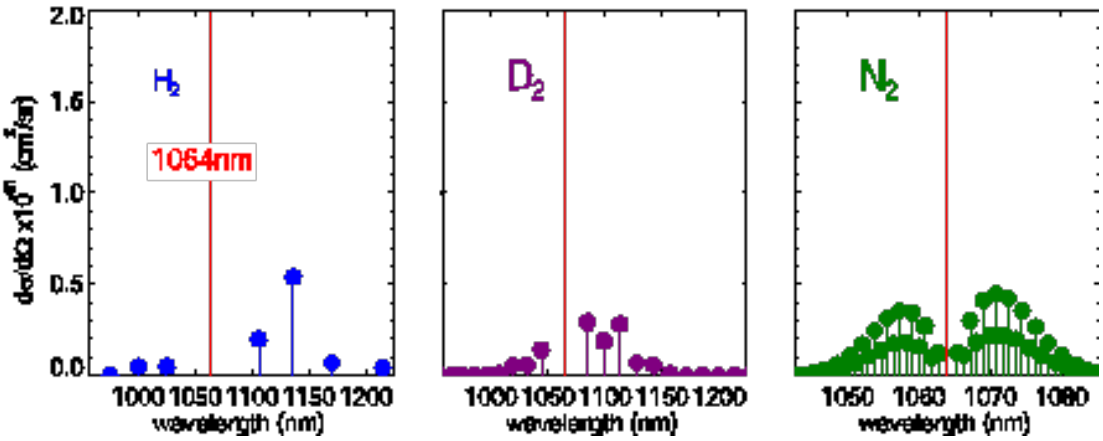

Figure 4.10: Raman spectra from 1064 nm excitation

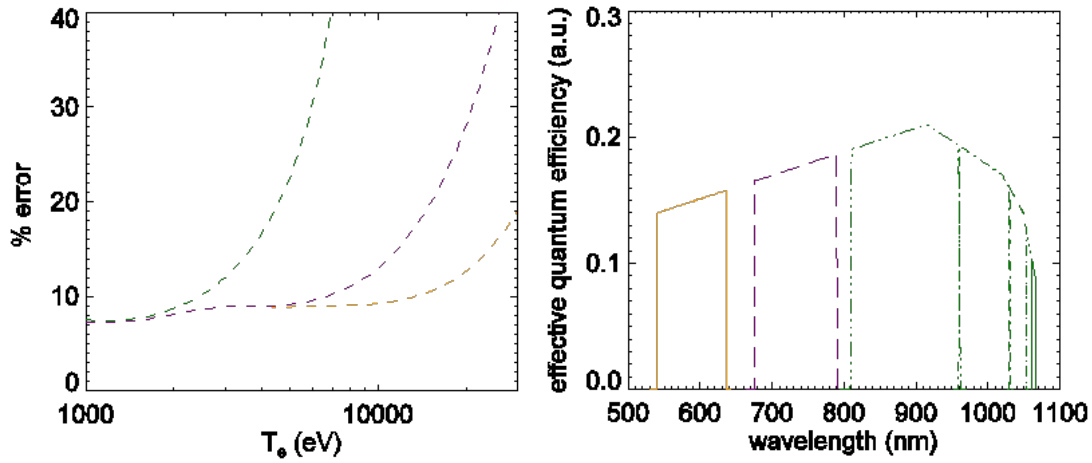

Figure 4.11: Potential spectral transmission bands and the fractional error on temperature resulting from the addition of various channels

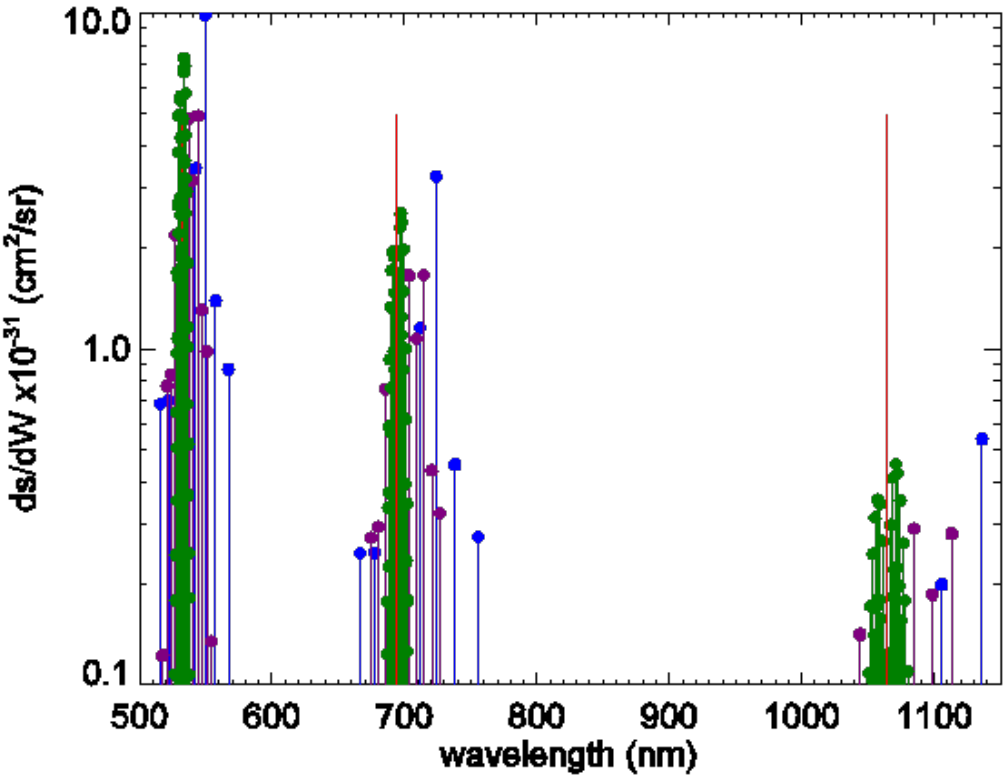

Figure 4.12: Example of Raman scattering for multiple lasers

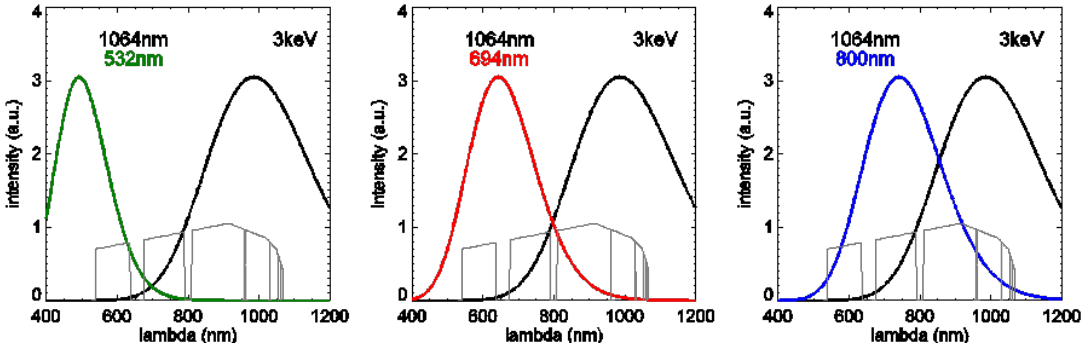

Figure 4.13: Examples of dual laser calibration

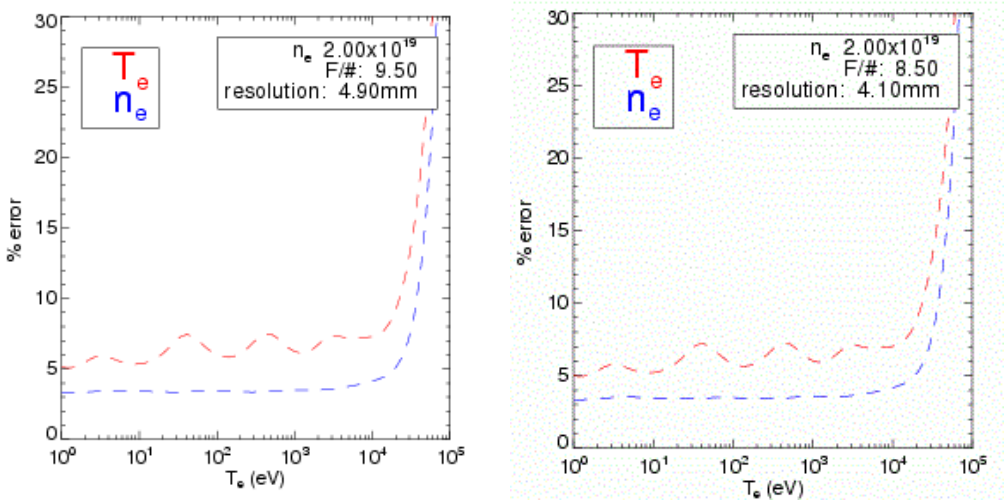

Figure 4.14: Performance of the edgeTS (a) for an edge point at the minimum density, (b) in the middle of the measured range, assuming the intermediate density where requirements on the error bars switch, (c) for the innermost point at the maximum density

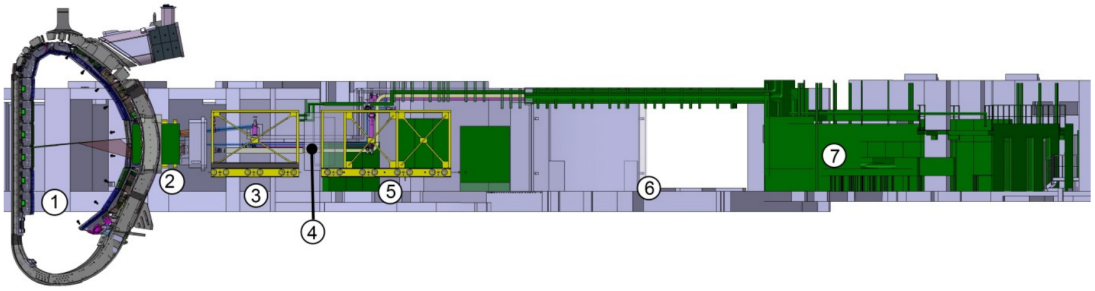

Figure 4.15: Distribution of Thomson scattering component in the ITER tokamak complex. 1)Plasma chamber; 2) Port Plug; 3) Interspace; 4)Bio-shield; 5) Port Cell; 6) Gallery; 7)Cell in Diagnostic Hall. The second confinement wall/barrier is between Port Cell and Gallery.

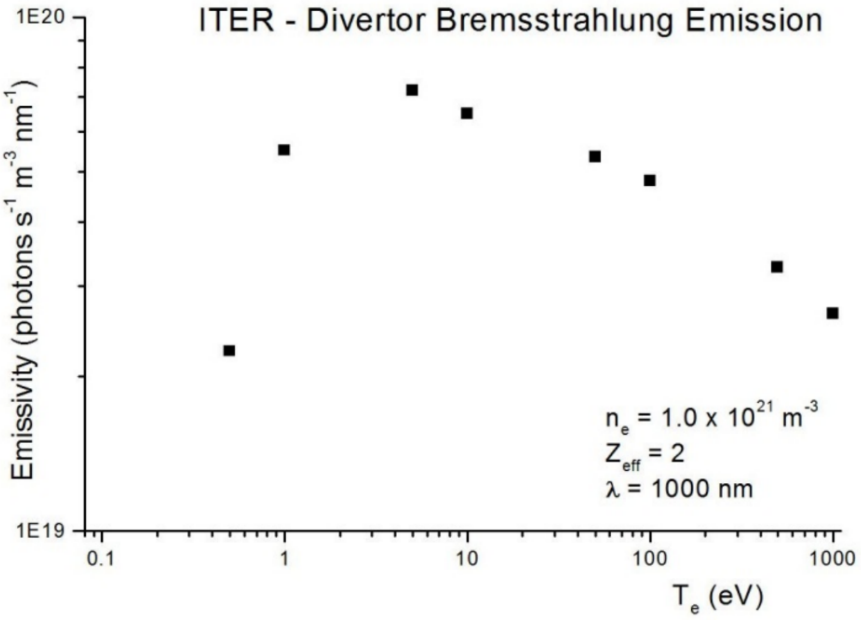

Figure 4.16: Emissivity of the divertor plasma at 1000 nm

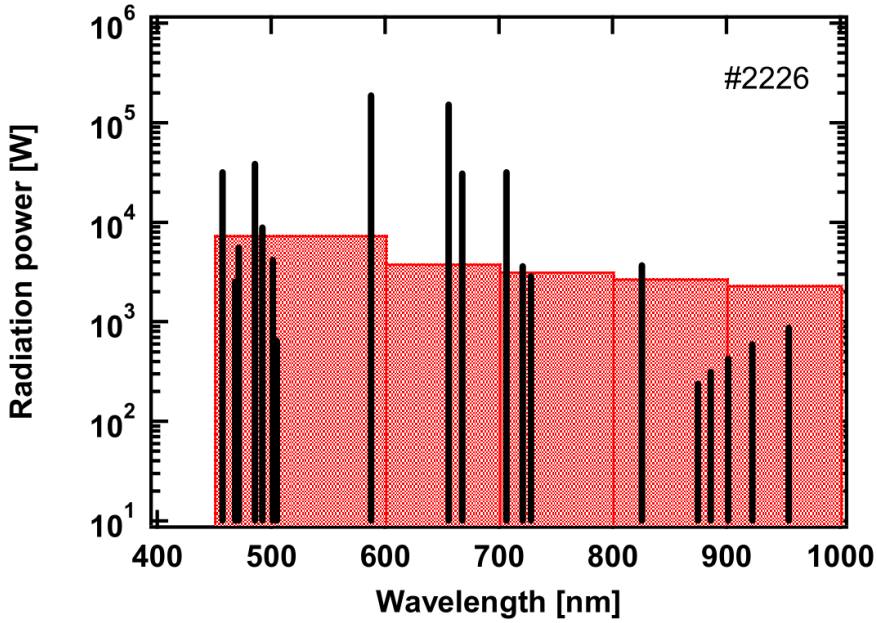

Figure 4.17: Radiation power for line emissions and bremsstrahlung emission (for case of power scenario #2226). Background continuum has been binned in 100 nm segments to compare the total power

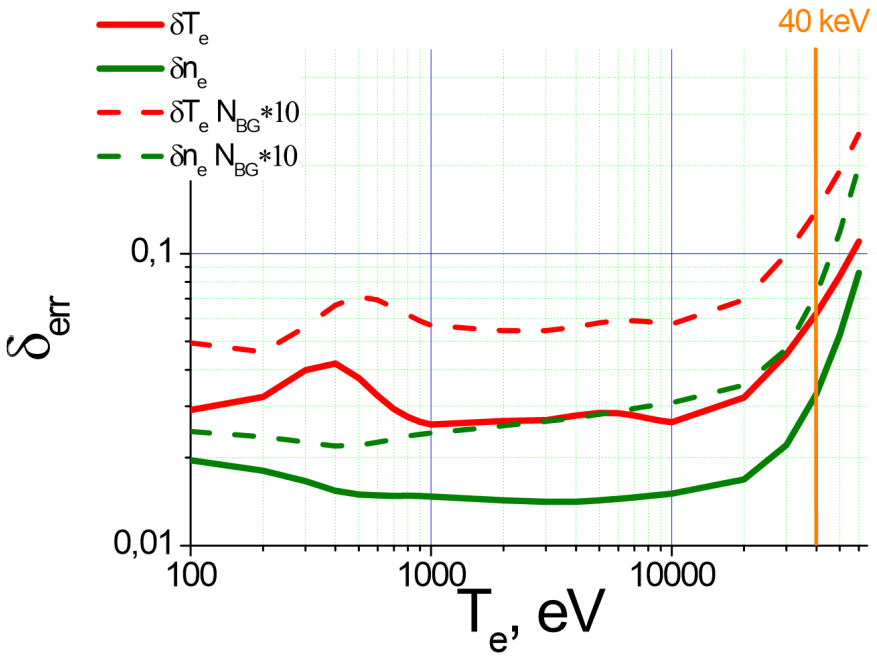

Figure 4.18: Laser energy 4 J, transmission is 50 % of the one which was estimated. The error curves are showing the value of 1σ, i.e. of an error bar that only provides a 66 % interval of confidence

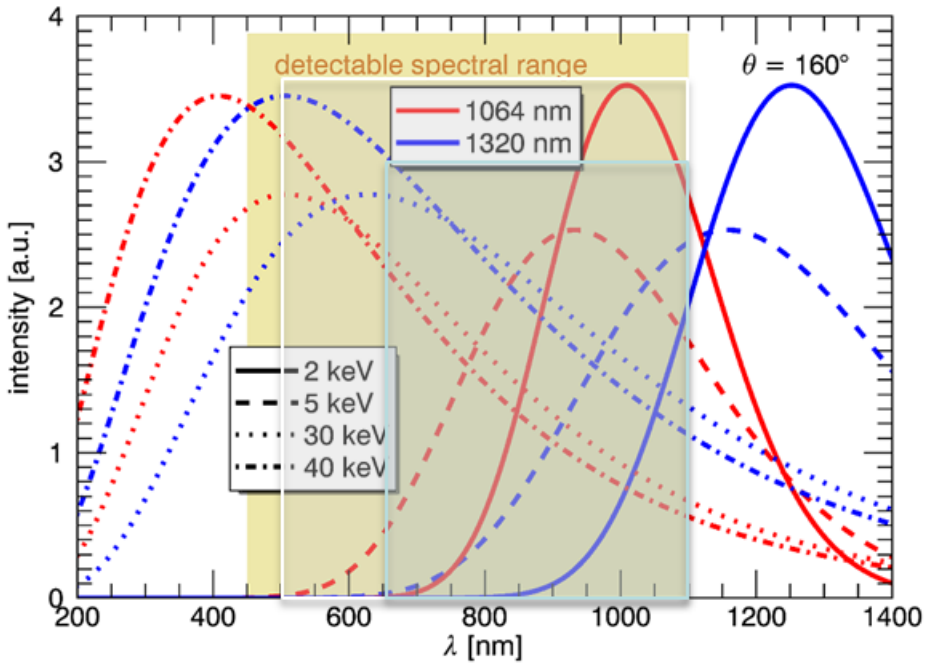

Figure 4.19: Scattering spectra are affected by the reduced transmission of fibres and M1 in the region 450-650 nm

5. Conclusion

High temperature plasma investigation is one of the main topics of current research since it could be the way to controlled fusion on Earth as a source of energy. However, investigation of such physical phenomena has been found very challenging due to the extreme conditions of the studied plasma. Tokamaks have approved to be a promising devices in our study of high temperature plasma. Tokamak COMPASS is trying to contribute to this effort. To fulfil this goal COMPASS has been equipped with set of many diagnostics and Thomson Scattering is one of them.

In the Introduction chapter, Thomson scattering theory is explained, including relativistic effects which play important role for the devices going towards fusion reactor. Concept of Thomson scattering diagnostic is introduced in following sections together with detail design of both COMPASS and ITER Thomson Scattering with all the specifics and issues.

This work also tries to improve how the errors of TS data are calculated. It describes different approaches to TS error estimation, since it is generally an issue of TS diagnostics and it is believed to be underestimated among many fusion devices and reasonable answer to this issue has not been found. Performance analysis and processing of COMPASS Thomson Scattering data are presented within published papers as an Appendix.

Bibliography

[1] R Aymar et al. Summary of the iter final design report. *ITER document G A0 FDR*, 4(01), 2001.

[2] Dustin H Froula, Neville C Luhmann Jr, John Sheffield, and Siegfried H Glenzer. *Plasma scattering of electromagnetic radiation*. Elsevier, 2011.

[3] M Hron, F Janky, J Pipek, J Sousa, BB Carvalho, H Fernandes, P Vondracek, P Cahyna, J Urban, R Paprok, et al. Overview of the compass codac system. *Fusion Engineering and Design*, 89(3):177–185, 2014.

[4] John D Lawson. Some criteria for a power producing thermonuclear reactor. *Proceedings of the Physical Society. Section B*, 70(1):6, 1957.

[5] O Naito, H Yoshida, and T Matoba. Analytic formula for fully relativistic thomson scattering spectrum. *Physics of Fluids B: Plasma Physics (1989-1993)*, 5(11):4256–4258, 1993.

[6] K Okamoto, K Toh, S Nagata, B Tsuchiya, T Suzuki, N Shamoto, and T Shikama. Temperature dependence of radiation induced optical transmission loss in fused silica core optical fibers. *Journal of nuclear materials*, 329:1503–1506, 2004.

[7] R Panek, J Stockel, J Havlicek, F Janky, M Hron, V Weinzettl, P Bilkova, M Dimitrova, P Hacek, R Dejarnac, et al. Characterization of ohmic and nbi heated h-mode in the compass tokamak. In *40th European Physical Society Conference on Plasma Physics*, pages 4–103, 2013.

[8] R Pasqualotto and A Alfier. Thomson scattering calibration with ultrabright supercontinuum light source. *Review of scientific instruments*, 77(10):10E502, 2006.

[9] SL Prunty. A primer on the theory of thomson scattering for high-temperature fusion plasmas. *Physica Scripta*, 89(12):128001, 2014.

[10] AC Selden. Simple analytic form of the relativistic thomson scattering spectrum. *Physics Letters A*, 79(5):405–406, 1980.

[11] J Stockel, R Panek, O Hronova, P Bilkova, V Fuchs, M Hron, P Pavlo, R Dejarnac, J Urban, V Weinzettl, et al. Reinstallation of the compass tokamak at ipp prague. 2008.

[12] V Weinzettl, R Panek, M Hron, J Stockel, F Zacek, J Havlicek, P Bilkova, DI Naydenkova, P Hacek, J Zajac, et al. Overview of the compass diagnostics. *Fusion Engineering and Design*, 86(6):1227–1231, 2011.

List of Tables

List of Abbreviations

APD	avalanche photodiode
CCD	charge-coupled device
DAQ	Data acquisition
eV	electron volts
F/#	F/ number (focal ratio)
Nd:YAG	neodymium doped yttrium aluminium garnet

Attachments